CONTRACT NO. 95-337
FINAL REPORT
MAY 1999

Measurement of the Ozone Concentration Aloft by Lidar During the Episode Monitoring Periods of the 1997 Southern California Ozone Study

CALIFORNIA ENVIRONMENTAL PROTECTION AGENCY
AIR RESOURCES BOARD
Research Division

Disclaimer

The statements and conclusions in this report are those of the NOAA/ERL/ETL and not necessarily those of the California Air Resources Board. The mention of commercial products, their source, and their use in connection with material reported herein is not to be construed as actual or implied endorsement of such products.

Mr. George, and Ms. Lisa Olivier, meteorologist. Ms. Gloria Schurman, secretary, processed an unusually large amount of paper work for the numerous person-trips to the field study site in a timely and accurate manner. Dr. Bob Weber, physicist, and Mr. David Welsh, computer specialist, in the ETL's System Demonstration and Integration Division (ET4) helped us in downloading meteorological data and other information in SCOS97 from the ET4's web site.

This report was submitted in fulfillment of Contract #95-337 entitled "Measurement of the Ozone Concentration Aloft by Lidar during the Episodic Monitoring Periods of the 1997 Southern California Ozone Study" by the National Oceanic and Atmospheric Administration's Environmental Technology Laboratory under the sponsorship of the California Air Resources Board. Special thanks are due to Mr. Leon Dolislager for his valuable help in providing important information for the background of this experiment and managing field operations; and for his critical review of the manuscript and many helpful suggestions. Work was completed as of May 1999.

Acknowledgments

Mr. Richard Marchbanks, optical engineer, re-designed the mechanical part of the two-dimensional scanner, re-coated the mirrors, and carried out miscellaneous hardware preparations. The new design significantly improved the stability of the scanner. During the 1997 Southern California Ozone Study (SCOS97) Experiment, Mr. Marchbanks was responsible for deploying the ozone lidar at the site, and took a major role in setting up, realignment, troubleshooting, and operation of the lidar. He was the only person in the crew that went to every episode in SCOS97. Mr. Keith Koenig, computer engineer, upgraded the lidar's data acquisition system. He installed new digitizer boards and a QNX operating system, re-wrote lidar operation programs for scanner control and raw data acquisition. He wrote programs for real time display of lidar raw data and real time display of preliminary ozone concentration and aerosol backscatter profiles, as well as various programs for on-site noise removing and system calibration to support the real time data analysis. The major improvement of the data acquisition system was the capability of real-time display that enabled the crew to view the current ozone and aerosol vertical structure, and thus helped them to make decisions about lidar operation (e.g., changing scanning parameters, lengthen working hours if the structure was interesting). Dr. Christoph Senff, research scientist, was one of the lead persons of the second-shift crew with an emphasis on science issues. His parallel post-processing of the data in the intercomparisons and the first two-days of the first episode in August 1997 provided a double check to the quality of data analysis. Dr. Wynn Eberhard, physicist, gave advice to the planning of the operation and managed the budget of the project. Ms. Kathleen Healy, computer analyst, set up a workstation in the lidar site to provide on-site data analysis. She re-wrote the tape reading and raw data averaging program, and wrote and modified all the data displaying programs in IDL language. Ms. Joanne George improved the plotting subroutine in the data analysis programs. She also modified a color table in the data display programs which covered a large dynamic range and thus allowed detailed structures and time variations of aerosol profiles to be well distinguished in color graphics. Mr. David Greenstone, student assistant, and Mr. Hutch Johnson, associate research scientist, were the major field support personnel. The field supporting crew also included Mr. Koenig, Ms. Healy,

TABLE OF CONTENTS

DISCLAIMER i

ACKNOWLEDGMENTS ii

TABLE OF CONTENTS v

LIST OF FIGURES vii

LIST OF APPENDICES ix

ABSTRACT xi

EXECUTIVE SUMMARY xiii

BODY OF REPORT

I. INTRODUCTION 1

II. THE ETL OZONE LIDAR 3

2.1 The lidar system OPAL 3

2.2 Improvements of the scanning system 8

2.3 Upgrades of the data acquisition system 8

2.4 Improvements of data analysis 9

III. LIDAR OPERATION IN SCOS97 11

IV. OZONE AND AEROSOL CONCENTRATIONS ALOFT AS MEASURED BY LIDAR DURING HIGH OZONE EPISODES . 13

V. SUMMARY AND DISCUSSIONS 19

REFERENCES 23

GLOSSARY OF TERMS, ABBREVIATIONS, AND SYMBOLS . . . 25

APPENDIX A 26

APPENDIX B 27

APPENDIX C 29

APPENDIX D 30

APPENDIX E 32

FIGURES

LIST OF FIGURES

Figure 1 Time-height charts of ozone concentrations and aerosol extinction coefficients at 355 nm during the episode of August 4-6, 1997

Figure 2 Time-height charts of ozone concentrations and aerosol extinction coefficients at 355 nm during the episode of September 3-7, 1997

Figure 3 Time-height charts of ozone concentrations and aerosol extinction coefficients at 355 nm during the episode of September 27-29, 1997

Figure 4 Time-height charts of ozone concentrations and aerosol extinction coefficients at 355 nm during the episode of August 22-23, 1997

Figure 5 Time-height charts of ozone concentrations and aerosol extinction coefficients at 355 nm during the episode of October 3-4, 1997

Figure 6 Time-height charts of ozone concentrations and aerosol extinction coefficients at 355 nm in the evening of August 4, 1997

Figure 7 Time-height chart of ozone concentrations and aerosol extinction coefficients at 355 nm during one scanning at about 2120 PST on August 4, 1997

Figure 8 Time-height charts of ozone concentrations and aerosol extinction coefficients at 355 nm from late afternoon to evening on September 5, 1997

Figure 9 Time-height chart of ozone concentrations and aerosol extinction coefficients at 355 nm during one scanning at about 1800 PST on September 5, 1997

Figure 10 Time-height charts of ozone concentrations and aerosol extinction coefficients at 355 nm in the evening on September 28, 1997

Figure 11 Time-height chart of ozone concentrations and aerosol extinction coefficients at

LIST OF APPENDICES

APPENDIX A	SCOS97's modeling domain of southern California and adjoining environs
APPENDIX B	Quotes from Reference 5: R. Lu and R.P. Turco, "Ozone distributions over the Los Angeles basin: 3-dimensional simulations with the SMOG model," *Atmospheric Environment* **30**, No. 24, pp. 4155-4176 (1996).
	(a) The model computation domain and topography
	(b) The simulation results on line A-A'
APPENDIX C	Lidar operation days in SCOS97
APPENDIX D	(a) Schematic figure of the lidar system OPAL
	(b) Optical layout of the transmitter and receiver of OPAL
APPENDIX E	Analysis on the statistical error in ozone concentrations

355 nm during one scanning at about 1720 PST on September 28, 1997

Figure 12 Time-height chart of ozone concentrations and aerosol extinction coefficients at 355 nm during one scanning at about 1820 PST on September 28, 1997

Figure 13 Time-height charts of ozone concentrations and aerosol extinction coefficients at 355 nm September 29, 1997

Figure 14 Time-height charts of ozone concentrations and aerosol extinction coefficients at 355 nm in three scanning operations at about 0620, 0720, and 0820 PST on September 29, 1997

ABSTRACT

In the SCOS97-NARSTO[1] field study the NOAA Environmental Technology Laboratory (NOAA/ETL)'s ozone profiling atmospheric lidar[2,3] (OPAL) was deployed in the Los Angeles urban area (El Monte Airport). During intensive operation periods (IOPs), OPAL operated continuously for more than 20 hours per day, providing vertical profiles of ozone and aerosol in an area important for understanding ozone evolution and transport, as well as for air quality model performance validation. In this 4-month long field campaign, OPAL detected persistent ozone and aerosol layers aloft on most days during the IOPs. Very frequently, a lower layer of ozone and aerosol at 1000-1500 m (msl) and a higher layer of ozone and aerosol at 2000-2500 m (msl) were observed by the lidar. These layers existed simultaneously during a time period from the late afternoon till midnight, when they started to dissipate. Sometimes, they persisted through the night and could be seen in the early morning.

EXECUTIVE SUMMARY

This final report describes the profiling of ozone and aerosol during the SCOS97-NARSTO field measurement campaign by the NOAA Environmental Technology Laboratory (NOAA/ETL)'s ozone profiling atmospheric lidar[2,3] (OPAL) in El Monte, CA.

OPAL transmits three ultraviolet (UV) wavelengths (266, 289, and 355 nm) in an eye-safe manner. The first two are for ozone profiling and the third is for aerosol profiling. The lidar has the unique capability of measuring profiles of ozone concentrations from near the surface to 2-3 km above the ground level and aerosol profiles up to 10 km. Prior to the SCOS97-NARSTO field study, a redesigned 2-dimensional scanner was installed on the lidar. The vertical scanning capability provides a valuable internal system check, enables frequent calibration, and permits analyses of horizontal variability in pollutant concentrations and of pollutant flux.

During intensive operational periods (IOPs) in the SCOS97-NARSTO field study, OPAL operated continuously for more than 20 hours per day, providing vertical profiles of ozone and aerosol in an area important for understanding ozone evolution and transport, as well as for air quality model performance validation.

The lidar was located at the El Monte Airport, about 15 km south of the foothills of the San Gabriel Mountains, which have a ridge line north of El Monte at altitudes about 2-2.5 km above mean sea level (msl). The intent of choosing this site was that the polluted air mass in the return flows from the San Gabriel Mountains could be detected by the lidar. The site elevation is 90 m (msl).

During the SCOS97-NARSTO field campaign, OPAL detected persistent ozone and aerosol layers aloft in the SoCAB. One layer was just above the top of the marine boundary layer, the other was at the same altitudes of the mountain ridge line north of the site. These layers existed simultaneously during a time period from the late afternoon till midnight, when

I. INTRODUCTION

Although ambient ozone concentrations have declined significantly as a result of major reductions in the emission of volatile organic compounds and nitrogen oxides, southern California continues to have the worst ozone problem in the United States. The complex meteorological and chemical processes taking place in the region are not fully understood. The 1997 Southern California Ozone Study (SCOS97) was planned to provide a new milestone in the understanding of relationships between emissions, transport, and ozone standard exceedances in southern California, as well as to facilitate modeling to refine estimates of the additional emission reductions required to attain the National Ambient Air Quality Standards. The study was conducted in coordination with the North American Research Strategy for Tropospheric Ozone (NARSTO). Thus, the field campaign is known as SCOS97-NARSTO.

The study's modeling domain of southern California and adjoining environs (see Appendix A) includes the rectangular area between approximately 32°N and 36°N latitude and between 115°W and 121°W longitude, an area of 205,000 square kilometers. The data collected are being extensively analyzed to determine how reductions in emissions might impact air quality, and also to quantify transport of pollutants between neighboring air basins.

The field activity started June 16 and ran through October 15, 1997. The existing monitoring network was supplemented with additional sites for the collection of continuous air quality and meteorological data. Moreover, during selected periods (generally, 2-3 days) when high ozone concentrations were forecast, additional monitoring and sampling occurred. During these intensive operational periods (IOPs), four to five aircraft, instrumented with ozone monitors and other monitoring equipment, made two to three flights per day; up to 75 balloon soundings were made per day; and additional samples of volatile organic compounds and carbonyls were taken.

As a high technology remote sensing instrument, the NOAA Environmental Technology Laboratory (NOAA/ETL)'s ozone profiling atmospheric lidar[2,3] (OPAL) was deployed in the Los

they started to dissipate. Sometimes, they persisted through the night and could be seen in the early morning. The continuous lidar observations during the intensive operational periods of SCOS97-NARSTO provided detailed temporal variations of ozone and aerosol vertical profiles that have never been available before. Further analysis of the lidar data, combined with wind and other observational data, will contribute significantly to the understanding of the formation and transport of the ozone layers, and bring new insight into important issues in air quality research in southern California.

II. THE ETL OZONE LIDAR (OPAL)

2.1 The lidar system and the principle of ozone remote sensing

OPAL is a differential absorption lidar (DIAL) system, which transmits three UV wavelengths (266, 289, and 355 nm) in an eye-safe manner. The first two are for ozone profiling and the third is for aerosol profiling. The innovative hardware design of this lidar makes it efficient, compact, and easily transportable.

A DIAL system transmits laser pulses at two wavelengths in an absorption band (or around a narrow absorption line) of the gas species under measurement. The wavelength with a higher absorption coefficient is called the "on-line" wavelength and the wavelength characterized by a lower absorption coefficient is called the "off-line" wavelength. Range resolution of a DIAL system depends mainly on the differential absorption coefficient of the wavelength-pair. Thus, proper selection of a wavelength pair is important to the range resolution (and the maximum detection range) of a DIAL system. The corresponding lidar equations at the two wavelengths take the form:

$$P_i(z) = C_{Ai}\frac{\eta_i(z)}{z^2}\beta_i(z)T_i^2(z), \qquad (1)$$

where the subscript i for various parameters in the equation stands for off-line (i = 1) and on-line (i = 2) wavelength, respectively; $P(z)$ is the detector-received power of the atmosphere-backscattered radiation (in Watts) from range z (in m), C_A is the instrument constant (in W m^3 sr), $\eta(z)$ is the overlap function, and $\beta(z)$ is the atmospheric volume backscattering coefficient (in m^{-1} sr^{-1}). $T^2(z)$ is the two-way atmospheric transmission, taking into account attenuation by molecular scattering, aerosol scattering, and ozone absorption,

$$T^2(z) = \exp\{-2\int_0^z [\sigma_m(z') + \sigma_a + \alpha_{o_3}\rho_{o_3}(z')]dz'\}, \qquad (2)$$

Angeles urban area. The lidar was located at the El Monte Airport, about 15 km south of the foothills of the San Gabriel Mountains, which have a ridge line north of El Monte at altitudes about 2-2.5 km (msl). The intent of choosing this site was that the polluted air mass in the return flows from the San Gabriel mountains could be detected by the lidar. The site elevation is 90 m (msl).

The objective of the OPAL measurements was focused on ozone layers aloft. Layers of high ozone concentrations aloft in the South Coast Air Basin (SoCAB) in California have been reported by many measurement projects. These layers may result from complex mesoscale flows in the basin, including sea breezes and thermally forced daytime up-slope flow in the mountains (so-called "chimney effect"). It is hypothesized that these high-concentration ozone layers aloft may contribute significantly to ozone standard exceedances in the basin by recycling pollutants from previous days, and/or increase ozone concentrations in downwind basins by transport. During IOPs, OPAL operated continuously for more than 20 hours per day, providing vertical profiles of ozone and aerosol in an area important for understanding ozone evolution and transport, as well as for air quality model performance validation. The lidar results showed very interesting ozone and aerosol layers aloft. One layer was always on top of the marine boundary layer, and the other at about the same altitude of mountain ridge line in the San Gabriel Mountains north of the site.

even higher. Using a larger Δz can reduce the relative error, assuming that δn is statistically constant. [A least-squared fit (either parabolic or linear) for the section of the curve, ΔlnF, can further improve the accuracy.] Thus, there is a trade-off between the accuracy of ozone concentration retrieval and the range-resolution. At far ranges, or after a layer of very high ozone concentrations and considerable thickness, the signal-to-noise ratio (SNR) decreases sharply. The signal decreases because of the decreasing two-way transmission $T^2(z)$, defined in Equation (2), and the reversed range-square effect in Equation (1). The relative increase in noise mainly originates from the inherent shot noise, which is a random fluctuation in photoelectrons and proportional to the square root of the signal, thus the SNR caused by this factor is proportional to $P/\sqrt{P} = \sqrt{P}$. Due to the decreasing SNR, we need to take a longer Δz to achieve a reasonable accuracy. But even so, the random error in retrieving ozone concentrations are still greater at far ranges. A detailed error analysis in ozone concentrations is described in Appendix E. Examples of error in ozone concentrations as a function of altitude are also plotted in Appendix E.

OPAL is an Nd:YAG-laser-based lower troposphere ozone lidar, specifically designed for measuring ozone in the boundary layer and the lower free troposphere. (See Appendix D for the schematic figure of the lidar and the optical layout of the transmitter and receiver.) This ozone lidar has unique features due to its innovative designs:

- **Range coverage**

The lidar has the capability of measuring ozone from near the surface (about 15 to 60 m) to about 3 km, allowing a complete ozone profiling in the boundary layer and in the lower free troposphere, whereas in other DIAL systems, the minimum detection range is typically 500 to 1000 m. This range-coverage is due to a multibeam transmitter[2,3] design that reduces the enormous dynamic range of the lidar signals (which is a typical feature of incoherent lidar systems), providing good signal-to-noise-ratio (SNR) in both near and far

where σ_m and σ_a are the extinction coefficients of molecules and aerosols, respectively; α_{o3} is the absorption coefficient of ozone, and ρ_{o3} is the ozone density.

Let $F(z) = P_1(z)/P_2(z)$, the off-line-to-on-line ratio of the lidar signals. Taking the logarithm and differentiating $ln[F(z)]$, we have

$$\frac{d}{dz}[\ln F(z)] = 2\Delta\alpha_{o3}(z)\rho_{o3}(z) + A(z), \tag{3}$$

where $\Delta\alpha_{o3}$ is the differential absorption coefficient of ozone, and

$$A(z) = \frac{d}{dz}\left\{\ln\left[\frac{\beta_1(z)}{\beta_2(z)}\right]\right\} + 2\Delta\sigma_m(z) + 2\Delta\sigma_a(z), \tag{4}$$

where $\Delta\sigma_m$ and $\Delta\sigma_a$ are respectively the differential extinction coefficients of molecules and aerosols. If the three terms in A(z) are properly estimated through aerosol data analysis, we can derive the ozone concentration ρ_{o3}

$$\rho_{o3} = \frac{\frac{dlnF(z)}{dz} - A(z)}{2\Delta\alpha_{o3}}. \tag{5}$$

In data processing, the differentiation $dlnF(z)/dz$ is calculated numerically. The interval of $dlnF(z)$ and z, i.e, ΔlnF and Δz, are finite, and the range interval Δz consists of more than one range gates. Thus the range-resolution of ozone concentrations retrieved from lidar signals is not the range gate of the signal digitizer, but related to the range interval Δz for carrying out the differentiation. Due to the presence of noise and signal fluctuation, the real data $\Delta lnF' = \Delta lnF + \delta n$, where δn is the noise difference at z and $z + \Delta z$. When Δz is small, ΔlnF is also small, thus the absolute value of error in ozone concentrations, i.e., $\delta n/\Delta z$, can be comparable to $\Delta lnF/\Delta z$, or

An off-axis paraboloid Newtonian telescope has been designed as the receiver. Special baffles in the telescope and an optical filter system in the detector package are employed for rejecting the daytime background radiation while keeping a high optical transmission for the receiving system. The receiver is assembled side by side with the transmitter on an invar optical board.

A data acquisition and processing system based on a PC is employed. Lidar output signals are digitized and pulse-to-pulse raw data are written on DAT tapes. The data files are first processed by a raw data averaging and display program. The output ASCII files are then processed with a sophisticated signal retrieval program to obtain ozone and aerosol profiles. The upgraded data acquisition system consists of a four-channel, 12-bit, 30 MHz digitizer, and a computer with both QNX and DOS operating systems, which enables a real-time display of the ozone lidar raw signals and the first-cut ozone profiles. Details are described in Section 2.3.

The lidar is installed in a well-insulated, temperature-controlled laboratory, modified from a 20-foot sea-container (seatainer). Because the laboratory has an air-bag cushioned floor and is mounted on an air-ride trailer, the lidar is transportable. The mobile laboratory has two compartments. The lidar is in the aft compartment; the computer and other instruments, cabinets and counters are in the forward compartment. There is an opening on top of the seatainer to allow lidar observations. A turning mirror set installed on the lidar optical board directs the horizontal laser beams up through the opening in the vertical direction, and also turns the atmosphere-backscattered radiation into the receiving telescope. A two-mirror scanning system is installed on top of the opening. The operation modes of the scanning system are: (1) steering the beams in the horizontal direction for system calibrations and horizontal measurements, (2) steering the beam in the vertical direction, and (3) scanning through elevation angles between 30-150° to make scanning measurements in one vertical plane.

Prior to the SCOS97-NARSTO field study, a redesigned 2-dimensional scanner was installed on the lidar. The vertical scanning capability provides a valuable internal system check,

ranges. The multibeam transmitter configuration requires a very high alignment accuracy and system stability. Very precise lateral transfer retroreflectors and a laser beam analyzer have been employed to assure the alignment accuracy. An invar optical table and a well-designed supporting system provide the needed system stability.

- **High optical efficiency and compact size**

The unique design of the detector package makes the optical efficiency very high (about 3 to 10 times higher than similar ozone lidar systems). In addition, the multibeam transmitter provides flat range response that allows a greater gain of the detectors to be employed. With these features the system has a modest laser pulse energy requirement and can use a small-sized telescope. Thus, the lidar is compact in size (~1 m^3) compared with similar systems.

With the multibeam configuration, four beams are output from the transmitter, three two-color beams at 266 and 289 nm (with energy allocation of 8%, 18%, and 74% among beam #1, 2, and 3), and one beam at 355 nm. The wavelength pair 266/289 nm has been chosen to obtain a high differential absorption coefficient, which provides the basis for high spatial and temporal resolution of the measurement. The online wavelength at 266 nm is obtained by frequency-quadrupling the fundamental wavelength of the YAG laser. The offline wavelength is produced by Raman shifting the frequency-doubled YAG output (at 532 nm) through a deuterium Raman cell to 632.5 nm, and then frequency-summing 532 and 632.5 nm to 289 nm through a nonlinear crystal. 532 nm was used in the 1993 Los Angeles Atmospheric Free Radical Study (LARFS) experiments for aerosol profiling. For eye-safety reasons, however, the channel was changed to 355 nm. The 355 nm is a product of frequency-tripling, by using the residual energy at 532 and 1064 nm. Thus, the transmitter is basically all solid state with wavelengths that are fixed, saving the lidar from problems usually associated with dye lasers. These three ultraviolet (UV) wavelengths are eye-safe for airplane pilots and passengers (the cutoff wavelength for airplane windows is at 375 nm).

higher than the old 12-bit digitizer.

- A QNX operating system was installed that allowed real-time display of the signal as well as the preliminary processed time-height ozone concentration and aerosol distributions.

- Preliminary calibration data could be processed on-site to support the real-time display of ozone concentrations and aerosol profiles.

- Upgraded lidar operational programs allowed more frequent system calibrations.

2.4 Improvements of data analysis

- System calibrations were frequently carried out through horizontal observations. The calculated system calibration functions were then checked with the surface ozone value and corrected if needed. The corrected calibration functions were smoothed to minimize the fluctuations caused by statistical noise. Moreover, a linear interpolation was used to calculate the calibration function for each lidar vertical or scanning file. These measures reduced the ozone concentration systematic error caused by any residual change in the scanner system to less than 2 ppb.

- Improved the algorithm and related program of removing the signal-induced fluorescence in the tail of the signals.

- A parallel processing of part of the data through two different programs provided internal comparisons, and the differences between ozone concentrations were mostly within 10 ppb.

- For scanning data at elevation angles other than 90°, ozone concentration ρ (or aerosol extinction coefficient σ) versus range, r, were transferred to ozone concentration or aerosol extinction coefficient) versus altitude, h, through the

enables frequent calibration, and was desired to address both monitoring and modeling issues.

The lidar has the unique capability of measuring profiles of ozone concentrations from the surface to 2-3 km above the ground level and aerosol profiles from 30-45 m up to 10 km. The raw data were recorded with a signal sampling interval of 5 m. With an averaging of 600-1200 pulses (5-10 min), the retrieval of ozone concentrations has a range resolution from a few tens of meters in the lower boundary layer to 150-200 m at about 3 km. Range resolution decreases with height because the signal-to-noise ratio is lower at farther ranges. The aerosol profiling at 355 nm has a maximum range of about 10 km with a range resolution of 15 m.

2.2 Improvements of the scanning system

The original 2-D scanning system developed in 1995 was re-designed. Major improvements included:

Redesign of the mirror mount, to minimize the mirror-warping effect during ambient temperature changes.

A sealed closure of the whole scanning system that keeps a better environment for the mirrors during the non-operation hours.

A better baffle system that blocks the light scattered by the mirrors from entering the receiver and the UV detection system (although in later episodes of the field study, because the mirrors became highly contaminated during the study, scattering from the mirrors was too strong to be fully blocked).

2.3 Upgrades of the data acquisition and operation system

The data acquisition system was upgraded. The major improvements were:

- The old one 8-bit, one 12- bit cards were replaced by two 12-bit, two-channel Gage digitizing cards. The sampling rates of the new digitizers were three times

III. LIDAR OPERATION IN SCOS97

OPAL was set up at El Monte Airport during June 2-11, 1997. It operated during five ozone intensive operational periods in SCOS97, i.e., (1) August 4-6, (2) August 22-23, (3) September 3-7, (4) September 27-29, and (5) October 3-4. The major episodes were the early August and late September IOP's, during which the surface ozone concentrations were well above the national 1-hour standard. Intercomparison experiments were carried out on June 11, and July 8. The total number of operational hours was about 350. A listing of the operational dates during SCOS97 is provided in Appendix C.

During the IOPs, OPAL operated continuously for 20 hours in a normal day (2 shifts of crew), beginning at 0300 PST, and ending at 2300 PST. When the vertical structure was interesting the operation continued through midnight. During a normal hour of operation, measurements consisted of 5 minutes for system calibration (horizontal orientation), 5 minutes for characterization of system noise, 12 minutes for scanning in a vertical plane, and 30-40 minutes for vertical profiling. When there were hardware problems or power blackouts, or some operator was testing, modifying, or adjusting software or hardware, lidar operation stopped, leaving small gaps in data taking. There were only one and half days (September 3-4, 1997) that the lidar was down due to a laser hardware failure. New parts were ordered, the lidar system was re-aligned, and the observation resumed in the morning of September 5.

Lidar operation was significantly improved through real-time display. The crew was able to view the current vertical distributions of ozone and aerosol. When higher ozone and/or aerosol layers aloft were observed (usually during the period of late afternoon to midnight), additional scanning operations were carried out to confirm the existence of the layers aloft. Real-time results inspired the scientists to have more ideas about future research in ozone formation and transport in the Los Angeles Air Basin.

As mentioned in Section II, system calibrations were frequently carried out through

equation $h(i) = r(i)sin\phi$, where h is the altitude, r is the slant range, i is the bin number of the slant range, and ϕ is the elevation angle. After this transfer, the altitude interval Δh is less than the slant range interval Δr , i.e., 15 m, by a factor of $sin\phi$. Thus the $\rho(h)$ and $\sigma(h)$ were interpolated between adjacent points to allow the altitude interval Δh to be 15 m, same as that in vertical data files. The resultant ozone profiles can then be plotted in time-height charts in a Cartesian coordinate, and thus avoid some artificial interpolation effect as found in the polar coordinate.

- Different color tables are used for ozone concentration and aerosol display to cover different dynamic ranges. Gaps were inserted in the graphics when data gaps existed, to avoid artificial interpolation in the contouring routine.

The improvements in scanner hardware, the frequent calibrations during operation, and improvements in data processing significantly reduced the systematic error caused by the system overlap function and the interference from the signal-induced fluorescence. The quality of the data retrieval are shown in scanning data displays, where the artificial curves caused by the system are removed, and horizontal layers of atmospheric ozone concentrations and aerosol extinctions are shown (see examples in Figures 7, 9, 11, 12, and 14).

IV. OZONE AND AEROSOL CONCENTRATIONS ALOFT AS MEASURED BY LIDAR DURING HIGH OZONE EPISODES

To display temporal and vertical variations in ozone and aerosol measurements, data for each day of the intensive monitoring periods during SCOS97-NARSTO were plotted in contoured time-height charts, and one chart a day in Figures 1-5. Time-height charts of ozone concentrations and aerosol extinction coefficients at 355 nm are plotted on Figures 1-3 for the three episodes of greatest interest, i.e., the first episode of August, and the first and second episodes of September, respectively. Figs 4-5 are the charts for the second episode of August and the episode in early October, respectively. For easy comparison, all data in one episode are plotted on one page, with the same time scale (0-24 PST) and altitude scale (0-2500 m msl), using the same color scale for ozone concentrations and aerosol extinction coefficients at 355 nm. The unit for ozone concentration is ppb, and the unit for aerosol extinction coefficient is 0.01 km^{-1}. Occasionally the highest values of ozone concentrations are beyond the scale, and thus small areas in the charts are plotted in white. In each figure page there are 4-6 charts. Time-height charts of ozone concentrations are in the upper row, and time-height charts of aerosol extinction coefficients at 355 nm are in the lower row. In this way the diurnal variation of ozone and aerosol profiles as well as the day-to-day change can be easily seen.

The time-height charts are created through programs written in IDL (Interactive Data Language). These programs read the time series (mostly 5 min interval) of one-dimensional ozone or aerosol data files into a two-dimensional array, each column of the array represents one vertical profile at a specific time. Then the programs call a standard routine, CONTOUR, in the IDL software package to draw contour lines at a constant interval. A color table is assigned to show ozone concentrations or aerosol extinction coefficients at different levels. In principle, contouring processing includes interpolation. To avoid interpolation through data gaps (which may cause artificial temporal variations), data sets containing such gaps were plotted in separate contoured sections before and after the gap. It can be seen in the figures, i. g., in Figure 3, time-height chart on September 28, 1997 contains two gaps.

horizontal observations, because the atmosphere is homogeneous or nearly so in the horizontal direction. However, the lidar site was near the fence of the airport and the ground level was 2 m lower than the nearby street, the scanner on top of the lidar trailer was only 2.4 m (8 feet) above the street level, exact horizontal measurement was impossible. The elevation angle was 1.6-1.8°, to keep the beams slightly higher than any ground objects (which was checked through a telescope). However, the horizontal observations were toward NNW direction where the terrain had a slope of about 1.1°. Thus the lidar beams were fairly parallel to the ground - only about few meters above the ground in the calibration range. In terms of AGL (altitude above ground), these observations were nearly "horizontal".

concentrations lay just above the top of the marine boundary layer. According to the temperature soundings, the top of the marine boundary layer decreased from about 800 msl at 1700 PST to about 500 m at midnight. The altitudes of this ozone layer aloft decreased simultaneously with the underlying boundary layer. This layer could still be seen in the early morning of August 6.

The lower ozone layer during the evenings of September 5 and 6 was also very interesting. Notice in Figure 2, the layer between 1000-1500 m had almost identical temporal and spatial variations in these two days. The layer started at about 16 PST, and ended at about 18-19 PST, with ozone concentrations higher than 100 ppb, and height increasing with time from 1000 m to 1500 m. There was another layer observed after the ending of the previous layer on September 5. It started from 18 PST and lasted till midnight. Ozone concentrations in this layer were lower, in the range of 70-80 ppb. The height of this layer increased from about 800 m to about 1400 m at midnight. It still could be seen in the early morning of September 6. Details of the evening of September 5 are plotted in Figure 8.

When high ozone concentrations were present in the lower layer, an aerosol layer was always observed at the same altitude, with very similar patterns of structures, as shown in the evening of August 4 (Figure 6), August 22 and 23 (Figure 4) , September 5 and 6 (Figure 2 and 8) , and the second episode of September (Figure 3).

Layers at Higher Altitudes

Ozone and aerosol layers often appeared at altitudes above 2000 m, mostly between 2000-2500 m. The strongest ozone layer at these altitudes that OPAL observed in SCOS97 was during the evening of August 4 (see Figure 6). Ozone concentrations in this layer were about 170 ppb when first observed. This layer lasted from 16 PST till midnight. The altitude of the layer started from about 3000 m, lowered to about 2200 m 19-20 PST, and increased again with time to about 2500 m at midnight. Ozone concentrations began to decrease after 21 PST, but still were higher than 100 ppb. Aerosol extinction coefficients at 355 nm in this layer were also very

In the SCOS97-NARSTO field study, the nearly continuous lidar observations revealed diurnal variations in urban Los Angeles area which were not observable in the past. The diurnal pattern in high ozone episodes seems fairly consistent in each episode. In this field study, OPAL detected persistent ozone and aerosol layers aloft during the IOP's. Usually there are two layers of ozone and aerosol layers aloft: one below 1500 m, the other above 2000 m.

Layers at Lower Altitudes

In early mornings, ozone concentrations were nearly zero in the surface layers, while aerosol extinction coefficients at 355 nm were high. Above this nightly boundary layer, around 500-1000 m there was always a layer with relatively high ozone concentrations. According to continuous measurements through the night, the morning layer was the leftover from the previous night. The altitude of this layer was often lower in the early episodes in August and early September, and higher in the episodes in late September and early October. Ozone concentrations in this layer increased after sunrise, and mixed down to the ground at noon time (12-14 PST). During noon time, the high ozone layer extended from the surface to 600-1000 m. After 14 PST ozone concentrations began to decrease in the lower part of the layer. But often ozone concentrations kept increasing in the upper part of the layer until near sunset (see charts of August 5 and 6 in Figure 1, charts of August 22 and 23 in Figure 4, and charts of October 3 and 4 in Figure 5). Ozone scavenging by nitric oxide emissions in the late afternoon and night was clearly indicated in the lower part of the boundary layer. The strengthening of ozone in the upper part might be caused by the return flow from the San Gabriel Mountains that injected polluted air into the top of the inversion layer.[5]

From late afternoon or early evening, a layer of higher ozone concentrations was always observed between 1000-1500 m. In the early evening on August 4, ozone concentrations in this layer were higher than 100 ppb. The layer lasted until midnight, when ozone concentrations decreased to the low 70s in ppb. In the mean time, the altitude of the polluted layer also decreased from 1500 to 1000 m. The details were plotted in Figure 6. This layer of high ozone

The most complicated multi-layer structures were observed on September 29 (Figures 13 and 14). It can be seen in Figure 13 that there were several layers below 1500 m in the morning, the uppermost two layers merged at 8 PST, and the lower layer merged with the boundary layer at about 10 PST. Then the upper layer curved down and to some extent mixed with the lower layer in the early afternoon, but the two-sublayer structure still remained. In the afternoon, the two layers separated again. But only in the upper part were the ozone concentrations high. In Figure 14, scanning data at about 0620, 0720, and 0820 PST were plotted to show the morning structures in detail.

These multiple structures in the lower layer may be caused by complicated structure in temperature profiles, as we saw in a previous experiment in the Los Angeles urban area (the LARFS experiment in 1993, in Claremont, CA).[8] They may also indicate complicated mountain return flows. Apparently the middle layer at 1500 m in Figure 9 is not just above the boundary layer, as modeled in Reference 5. The formation of polluted air in different layers in late afternoon might be caused by return flows off mountains with different heights. These returns flows may have different directions, because the mountains have slopes facing the sea-breeze and sun at different angles. Thus, the complex layering structure of the atmosphere could also be a result of the complex local and mesoscale meteorological processes.

(This page intensionally left blank.)

V. SUMMARY AND DISCUSSIONS

Layers of high ozone concentrations aloft in the South Coast Air Basin (SoCAB) in California have been reported by many measurement projects. These layers may result from complex mesoscale flows in the basin, including sea breezes and thermally forced daytime up-slope flow in the mountains.

It is hypothesized that these high-concentration ozone layers aloft may contribute significantly to ozone standard exceedances in the basin by recycling pollutants from previous days, and/or increase ozone concentrations in downwind basins by transport.[4,5] During the 1987 Southern California Air Quality Study experiment, trajectory studies in two cases showed an upper level recirculation in the middle of the SoCAB.[6]

During the SCOS97-NARSTO field study, NOAA/ETL's OPAL detected persistent ozone and aerosol layers aloft in the SoCAB. In most cases one layer was just above the top of the marine boundary layer, the other was approximately at the altitudes of the mountain ridge line north of the site. More complicated multi-layer structures were often observed in early morning or in the evenings below 1500 m msl. The co-location of the ozone and aerosol layers implies that they probably originated from the same sources and processes. The modeling of Lu and Turco in Ref. 5 has a transect line that passes near El Monte, i.e., A-A' [See APPENDIX B (a)]. The simulated ozone concentrations at three different times of the day are plotted in three figures in APPENDIX B(b). These figures indicate the interactions between the sea-breeze and the San Gabriel Mountains. Two layers of ozone are formed aloft from the return flows off the San Gabriel Mountains: one layer was injected into the top of the inversion layer at about 1000 m, the other comes from the mountain top and has its center located at about 2500-3000 m. At 1600 PST, the two layers can both be seen at a distance about 30 km from the coast. This is very similar to what we observed at El Monte. However, lidar observations often detected a layer a few hundred meters above the marine boundary layer, and sometimes with more complicated structures. There might be multiple inversion layers (or thermally stable layers) in temperature

profiles that cause this complexity. Return flows off mountain tops at different altitudes with different azimuths might be another possible cause. Further analysis of the lidar data in conjunction with meteorological data from the collocated RWP/RASS profiling system and air quality data obtained from occasional aircraft spirals at El Monte should improve our understanding of the atmospheric processes. Moreover, we strongly recommend, in the future, a joint observation study of the powerful ETL Doppler lidar (i.e., the ETL's TEACO, which can measure the 3-D wind field in a large area) and the ozone lidar. Working together, these remote sensing technologies provide much more insight into the formation and evolution of polluted air layers. These improved insights into the mechanisms and processes contributing to the exceedance of the ozone standards in the SoCAB and surrounding areas will improve the technical basis of attainment plans.

Ozone scavenging is indicated by the decrease of ozone concentrations mainly near ground level. In the layers aloft, the trends of ozone concentrations and aerosol extinction coefficients at 355 nm in the evenings were often opposite to each other: ozone concentration decreased with time, while aerosol extinction coefficients at 355 nm increased. After sunset, when the photochemical production of ozone stopped, the scavenging and dispersion processes continued. NO_2 was created when ozone was scavenged by nitric oxide emissions. Various nitrogen compounds (e.g., NO_2, N_2O_5) and radicals act as reservoirs of potential oxygen atoms which are necessary for the formation of ozone. Any such compounds available in the following morning would enhance ozone formation after sunrise. The increase of the 355-nm extinction coefficient with time at night from the surface to 3 km may imply an increase in the aerosol size due to the increase in relative humidity at night. Because 355 nm is close to the peak of an NO_2 absorption band, a portion of the increase in the extinction coefficient may also be attributed to additional absorption by NO_2. However, the NO_2 absorption would only be about 10-20% of the 355-nm aerosol extinction coefficients, even if we assume NO_2 concentrations were as high as 100 ppb.

During daytime, ozone concentrations increased after sunrise in the boundary layer and

the layers aloft due to the photochemical processes that produce ozone. In the late afternoon ozone concentrations decreased in the lower part of the boundary layer due to the scavenging by NO and advection of cleaner air with the sea-breeze. Aerosol extinction coefficients at 355 nm had similar temporal variations in daytime as that of ozone concentrations. The similar temporal variations might be attributed to the production of smog aerosols in high ozone layers.

The continuous lidar observations during high ozone episodes in this field study provided time variations of ozone and aerosol vertical profiles that have never been available previously. Further analysis of the lidar data, combined with wind and other observational data, would contribute significantly to the understanding of the formation and transport of the ozone layers, and bring new insight into important issues in air quality research in Southern California.

(This page intensionally left blank.)

REFERENCES

1. E. M. Fujita, J. Bowen, M. C. Green, and H. Moosmüller (1997 draft), 1997 Southern California Ozone Study (SCOS97) Field Study Plan. Report prepared by Desert Research Institute for California Air Resources Board, Sacramento, CA. Contract No. 93-326.

2. Yanzeng Zhao, J. N. Howell, and R. M. Hardesty, "Transportable Lidar for the Measurement of Ozone Concentration and Aerosol Profiles in the Lower Troposphere," A&WMA/SPIE *International Symposium on Optical Sensing for Environmental Monitoring*, October 11-14, 1993, Atlanta, Georgia, pp.310-320.

3. Yanzeng Zhao, Richard D. Marchbanks, and R. M. Hardesty, "ETL's Transportable Lower Troposphere Ozone Lidar and Its Applications in Air Quality Studies, " 42nd SPIE Annual meeting, 31 July 1 - 1 August, 1997, San Diego, California, *Application of Lidar to Current Atmospheric Topics II,* Proceedings of SPIE #3127, pp.53-62.

4. J. L. McElroy and T.B. Smith, "Creation and fate of ozone layers aloft in southern California," *Atmospheric Environment* **27A**, No. 12, pp. 1917-1929 (1993).

5. R. Lu and R.P. Turco, "Ozone distributions over the Los Angeles basin: 3-dimensional simulations with the SMOG model," *Atmospheric Environment* **30**, No. 24, pp. 4155-4176 (1996).

6. S. G. Douglas, R. C. Kessler, C. A. Emery, and J. I. Burtt, "Diagnostic Analysis of Wind Observations Collected During the Southern California Air Quality Study," final report, prepared under Contract No. A832-133 for California Air Resources Board, Sacramento, CA, by Systems Applications International, San Rafael, CA (1991).

7. Y. Zhao, R. D. Marchbanks, C. J. Senff, H. D. Johnson, and Leon Dolislager, "Lidar

Profiling of Ozone and Aerosol in the SCOS97-NARSTO Experiment," 19th International Laser Radar Conference, July 6-10, 1998, Anapolis, Maryland.

8. Yanzeng Zhao, John A. Gaynor, and R. Mike Hardesty, "Demonstration of a New and Innovative Ozone Lidar's Capability to Measure Vertical Profiles of Ozone Concentration and Aerosol in the Lower Troposphere," Final Report to California Air Resources Board, Contract No. 92-328, December 1994.

GLOSSARY OF TERMS, ABBREVIATIONS, AND SYMBOLS

LIDAR	**Li**ght **D**etection **a**nd **R**anging (Lidar is a system that transmits laser beam(s) and collects backscattered radiation through telescope(s). The received radiation is then transferred to electronic signals by optical detectors. Since the backscattered radiation from different distances has different time delays, the signal is range-resolved.)
DIAL	**Di**fferential **A**bsorption **L**idar
RASS	**R**adio **A**coustic **S**ounding **S**ystem
RWP	**R**adar **W**ind **P**rofiler
NOAA	**N**ational **O**ceanic and **A**tmospheric **A**dministration
ETL	**E**nvironmental **T**echnology **L**aboratory (former Wave Propagation Laboratory)
PST	**P**acific **S**tandard **T**ime
AGL	**A**bove **G**round **L**evel
MSL	**M**ean **S**ea **L**evel

APPENDIX A

SCOS97's modeling domain of southern California and adjoining environs: an area of 205,000 square kilometers (downloaded from the NOAA/ETL/ET4 web site). The lidar site was collocated with a RWP system at El Monte (No. 12 on the map).

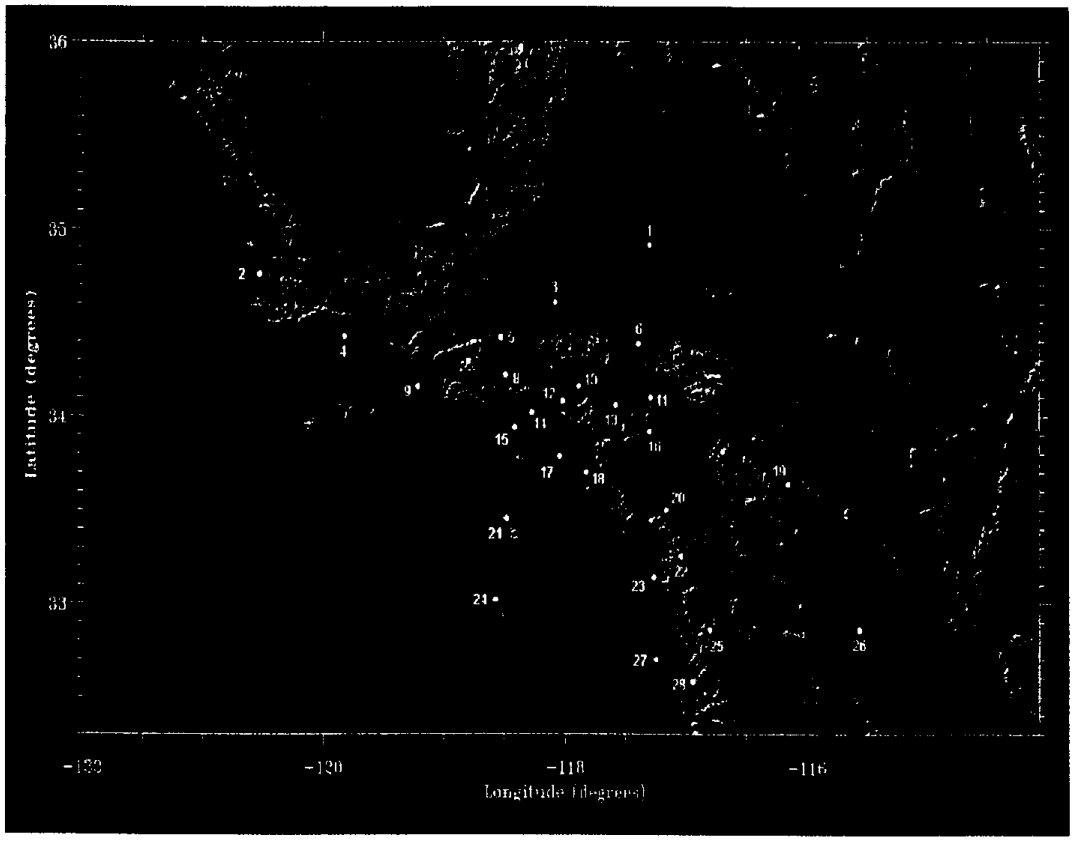

APPENDIX B

Quotes from Reference 5: R. Lu and R.P. Turco, "Ozone distributions over the Los Angeles basin: 3-dimensional simulations with the SMOG model," *Atmospheric Environment* **30**, No. 24, pp. 4155-4176 (1996).

(a) The model computation domain and topography

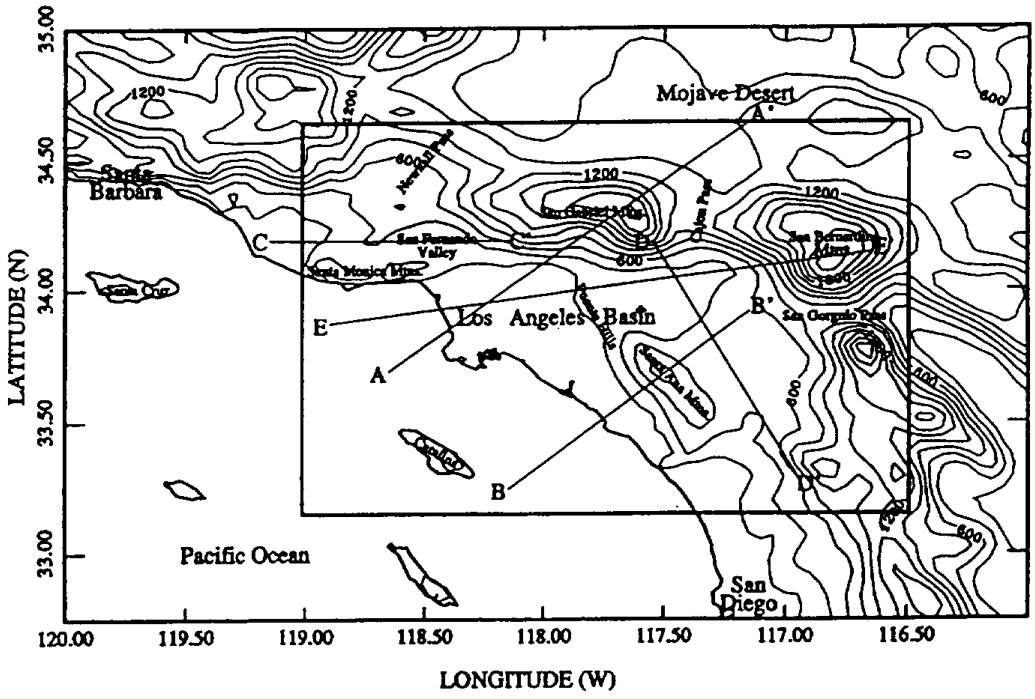

Fig. 1. The model computational domain and topography are illustrated. The larger map defines the area over which mesoscale dynamical calculations are carried out. The inner perimeter indicates the domain used for the air quality (chemistry and microphysics) simulations. Heavy solid lines indicate the coastline. Contour lines correspond to terrain elevations; the contour intervals are 200 m. The lines AA', BB', CC', DD' and EE' give the locations of the vertical cross-sections discussed in the text.

APPENDIX B (Continued)

(b) The simulation result of ozone concentration along line A-A'

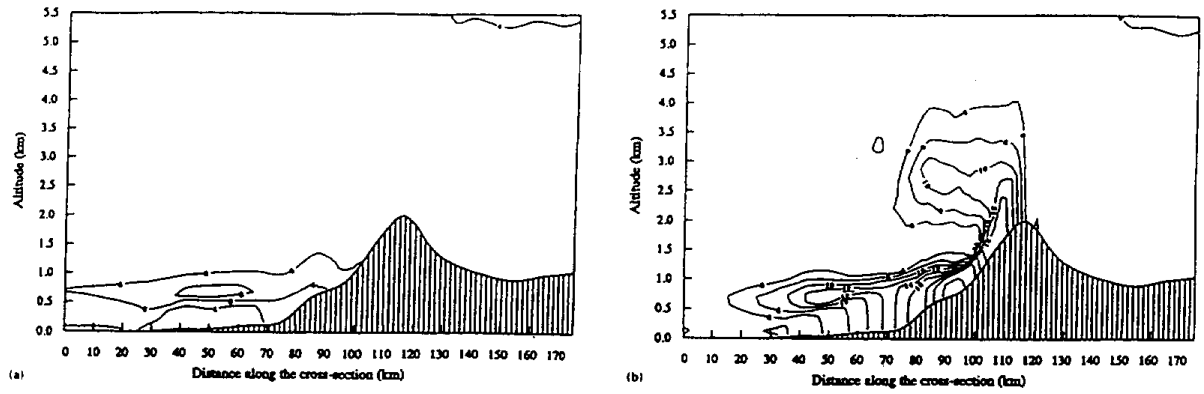

Fig. 4. Calculated ozone concentrations (contours, in intervals of 2 pphmv) for a vertical cross-section that extends from Santa Monica Bay to the San Gabriel Mountains (AA' in Fig. 1) on 27 August 1987. The topography is highlighted by striping. (a) 10:00 PST; (b) 14:00 PST.

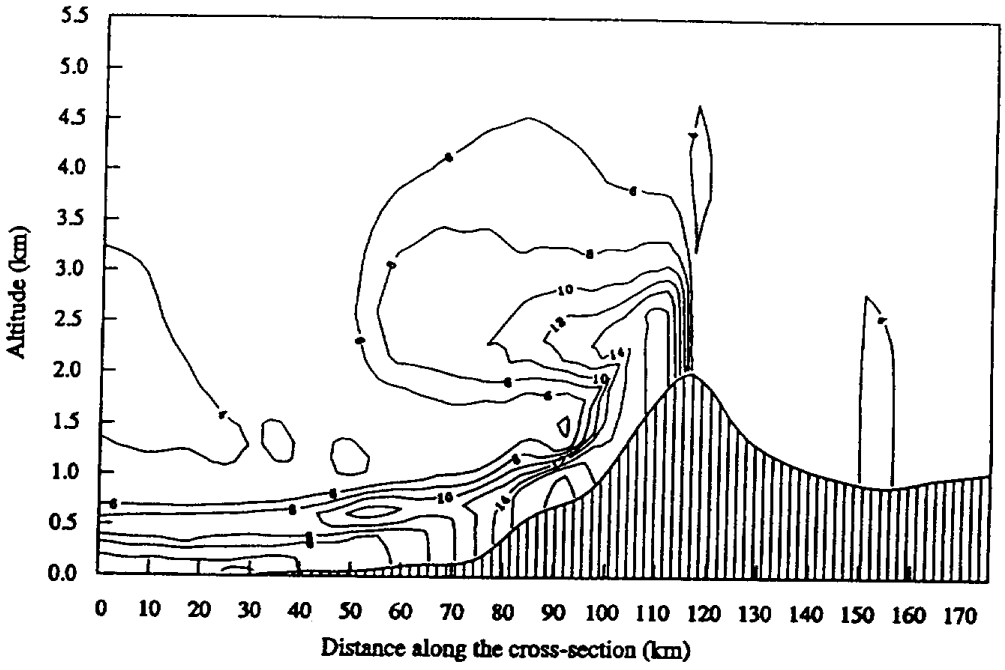

Fig. 6. Simulated ozone concentrations (contours, in intervals of 2 pphmv) for vertical cross-section AA' (Fig. 1) extending from Santa Monica Bay to the San Gabriel Mountains at 16:00 PST on 28 August 1987.

APPENDIX C

List of Lidar Operational Dates in SCOS97-NARSTO:

June 2-10, Set up and testing

June 11, 1997 - Intercomparison I

July 8, 1997 - Intercomparison II

August 4-6, 1997

August 22-23, 1997

August 24 (4 hours)

September 3 (4 hours) and September 5-7, 1997

September 27-29, 1997

October 3-4, 1997

APPENDIX D

(a) Schematic figure of the lidar

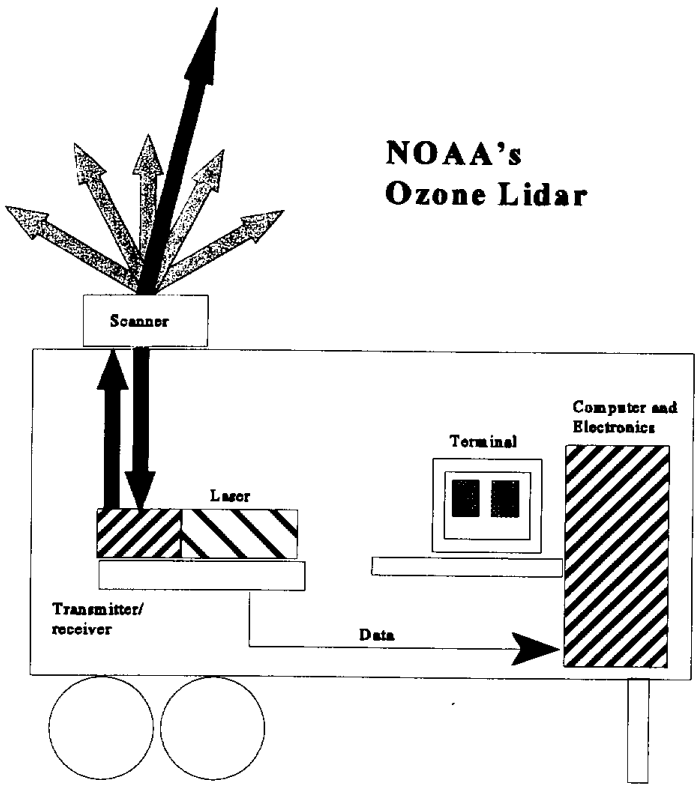

APPENDIX D (continued)

(b) Optical layout in the transmitter and receiver

Optical Layout of the Modified Transmitter

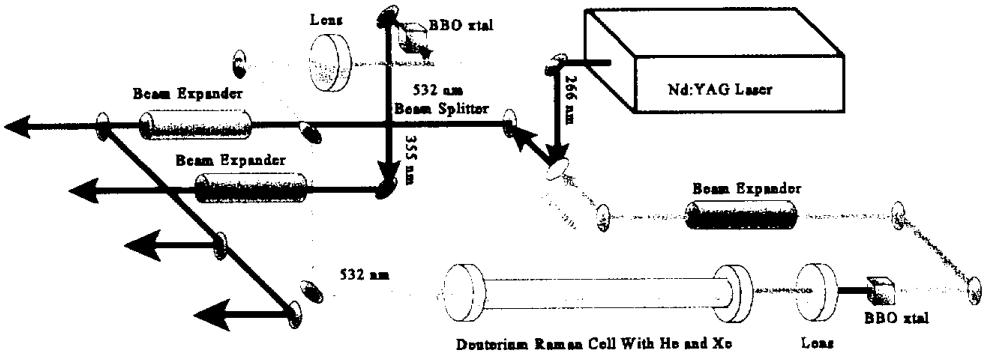

Optical Layout of the Detector Package

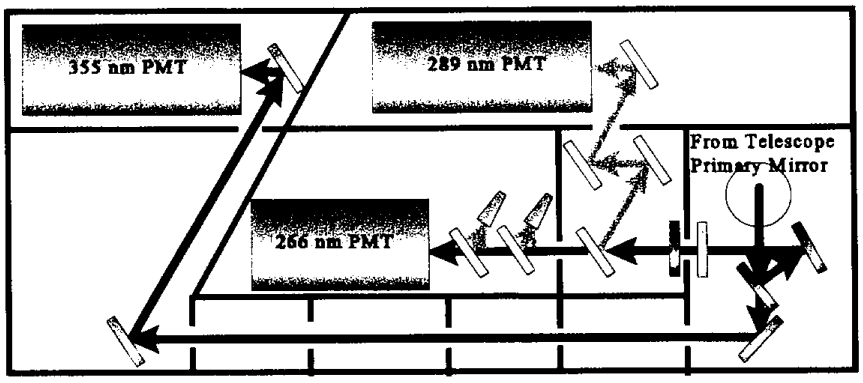

APPENDIX E Analysis on the statistical error in ozone concentrations

Ozone concentrations are calculated using Eq. (5) in Section II (The ETL Ozone Lidar) of the final report. A differentiation of the logarithm ratio $lnF(z)$ needs to be carried out numerically. Ozone concentration is proportional to the slope of $lnF(z)$, i.e., $d\,lnF(z)/dz$, which is statistically estimated using least square methods. The following is a detailed derivation of the variance and the standard deviation of the slope, and the resulting statistical errors in ozone concentrations.

1. Linear least square fit

Using linear least square method to fit y in a range interval from $z = z_1$ to z_2, where $z_1 = \bar{z} - k\Delta z$, $z_2 = \bar{z} + k\Delta z$, $\bar{z} = (z_1 + z_2)/2 = z_i$, the range at the i^{th} sample point, Δz is the range gate of the digitizer, and $2k+1$ is the total number of sample points used in the least square fit. The linear estimate of $ln[F(z)]$, y, is a linear function of range z:

$$y = a + b(z - \bar{z}). \tag{1}$$

The variance of the slope b is

$$\sigma^2 = \frac{s^2(y)}{\sum_{j=-k}^{k}(z_{i+j} - z_i)^2} = \frac{s^2(y)}{(\Delta z)^2 \sum_{j=-k}^{k} j^2} = \frac{s^2(y)}{2(\Delta z)^2 \sum_{j=1}^{k} j^2}, \tag{2}$$

where $s^2(y)$ is the variance of y, defined as: $s^2(y) = \frac{1}{2k-1}\sum_{j=-k}^{k}(Y_{i+j} - y_{i+j})^2$, where Y is the data and y is the least square fit. Therefore, the root-mean-square of the slope b is

$$\sigma = \frac{s(y)}{\Delta z\sqrt{2\sum_{j=1}^{k} j^2}}. \tag{3}$$

It is proportional to the root-mean-square (standard deviation) of y, and inversely proportional to the standard deviation of the range. That means the accuracy of the estimate of the slope increases with smaller standard deviation of noise and greater range interval.

2. Parabolic least square fit

The parabolic least square fit curve has the form

$$y = a + b(z - \bar{z}) + c(z - \bar{z})^2. \tag{4}$$

The slope $\frac{dy}{dz}$ at $z = \bar{z} = z_i$ is b, which can be calculated by the following equation:

$$b = \frac{\Delta z\sum_{j=1}^{k} j[y(z_{i+j}) - y(z_{i-j})]}{2(\Delta z)^2\sum_{j=1}^{k} j^2} = \frac{\sum_{j=1}^{k} j[y(z_{i+j}) - y(z_{i-j})]}{2\Delta z\sum_{j=1}^{k} j^2}. \tag{5}$$

The variance of b is then

$$\sigma^2 = \frac{\sum_{j=1}^{k} 2j^2 s^2(y)}{\left[2(\Delta z)^2\sum_{j=1}^{k} j^2\right]^2} = \frac{s^2(y)\left[2\sum_{j=1}^{k} j^2\right]}{\left[2(\Delta z)^2\sum_{j=1}^{k} j^2\right]^2} = \frac{s^2(y)}{2(\Delta z)^2\sum_{j=1}^{k} j^2}, \tag{6}$$

It is interesting to see that Eq. (6) is the same as Eq. (2), i.e., at $z = \bar{z} = z_i$ the variance of the estimated slope has the same mathematical expression for linear or parabolic fitting. However, with a better least square fit, the standard deviation of y will be smaller and the slope will have higher accuracy.

3. Error in the ozone concentration due to the statistical uncertainty of the slope

It is straightforward to calculate the statistical error in ozone concentration caused by the uncertainty in the slope of $ln[F(z)]$. Using Eq. (5) in Section II of the final report, we can easily obtain the standard deviation of ozone concentration

$$\sigma(\rho_{O_3}) = \pm \frac{\sigma}{2\Delta\alpha}. \qquad (7)$$

When estimating the error in ozone concentrations, we multiply $\sigma(\rho_{o3})$ by a factor of 2 to have 95% of the error estimates within this range.

Implementing the equations in our programs but keeping the other parameters unchanged, we reprocessed part of the data files on September 28, 1997, to obtain the statistical errors of ozone as a function of altitudes at different times of the day when signal-to-noise ratios (SNR) varied. In order to see the effect of decreased transmitted laser energy on the statistical errors in ozone concentrations, a part of the data in the evening of August 4, 1997 was also reprocessed.

The statistical error will be higher when the signal is lower. As shown in Eq. (1) in Section II, the signal $P(z)$ is proportional to the atmospheric transmission (related to the attenuation by ozone and aerosol), the aerosol backscattering coefficient, and the instrument constant (which is proportional to the transmitted laser energy). The late September episode was the last major IOP in the SCOS97 field campaign. The scanning mirrors were seriously damaged by the pollution. The errors in ozone concentrations in the evening of August 4, 1997 (the first day of the first major IOP) were two times smaller (less than 5 ppb throughout most of the

detection range) than those in the evening of September 28, 1997 (compare Figure A and Figure E). This implies an energy loss by a factor of about 4 due to the decrease of reflectivity in the scanning mirror coatings. In fact, in the last day of the experiment, we took off the mirrors and found that the signals immediately increased by a factor of 5. Therefore, the errors calculated for data taken on September 28 should be the upper limits of those during the field study.

Errors in ozone concentrations at different altitude ranges at different times during the day of September 28 (especially those with higher errors) are listed in Table 1, and examples of the error profiles are plotted in Figures A-E. The errors are low from late evening to the next morning throughout the measurement range. At altitudes above 1000-1500 m, the errors increase fast from mid morning to noon, reaching a maximum in early afternoon when ozone concentrations in the boundary layer were highest for the day. During this short time period (about one hour), ozone data above ~1500 m have errors of approximately 25 ppb or more and thus may not be usable. But in the boundary layer (below ~1000 m), the statistical errors in ozone concentrations remains less than 10 ppb.

Table 1. Statistical error in ozone concentration retrieval from lidar data (Examples during 9/28/1997)

0054-0119 PST		1229-1259 PST		1327-1407 PST		1429-1454 PST		1729-1754 PST	
MSL(m)	2σ (ppb)	MSL(m)	2σ (ppb)	MSL(m)	2σ (ppb)	MSL(m)	2σ (ppb)	MSL(m)	2σ (ppb)
0-1000	2-5	0-1000	1-8	0-800	3-8	0-1000	1-8	0-1000	1-6
1000-1500	3-5	1000-1200	8-15	800-1000	8-23	1000-1500	6-10	1000-1500	2-6
1500-2000	5-9	1200-1600	15-20	1000-1500	20-25	1500-1700	15-20	1500-2000	6-12
2000-2500	7-11	> 1600	> 25	>1500	> 25	1700-1900	20-25	2000-2500	12-16

The low accuracy in high altitudes at noon time were primarily due to the low signal level when laser beams and backscattered radiation traveled through a thick layer of high ozone concentrations (about 200 ppb during that time period), and also may be due to the damage of the scanning mirrors which remained in the polluted air of Los Angeles for four months. These errors presented are among the worst during SCOS97. We are now improving the far-range

signals of OPAL by adding another wavelength. The range resolution will be lower as a trade-off for longer range ozone monitoring when ozone concentrations in the boundary layer are high.

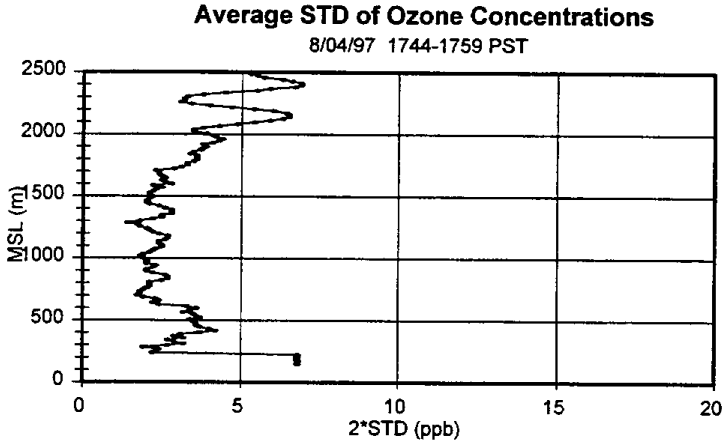

Figure A

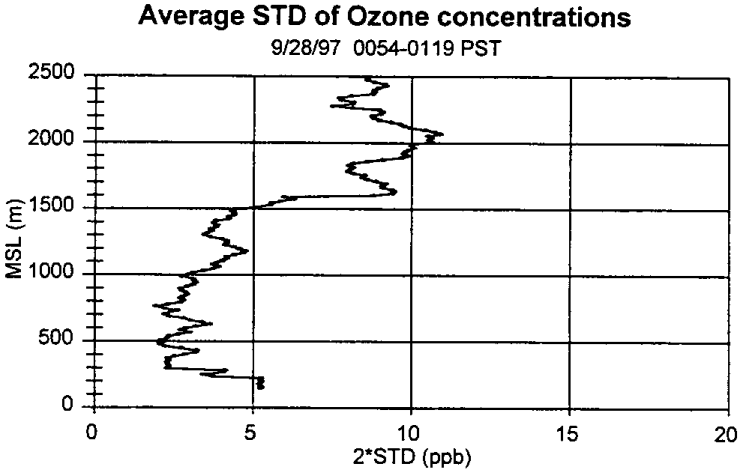

Figure B

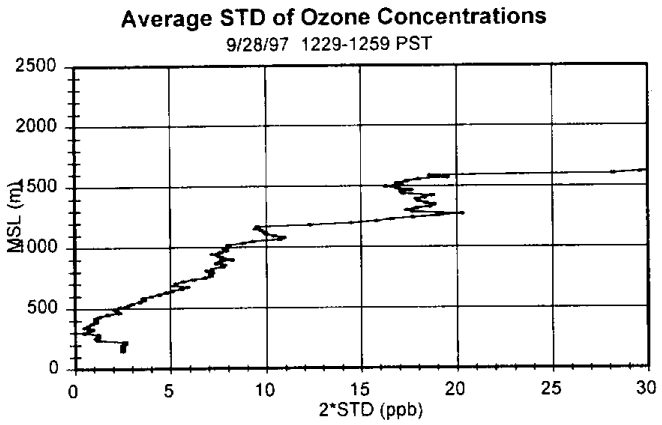

Figure C

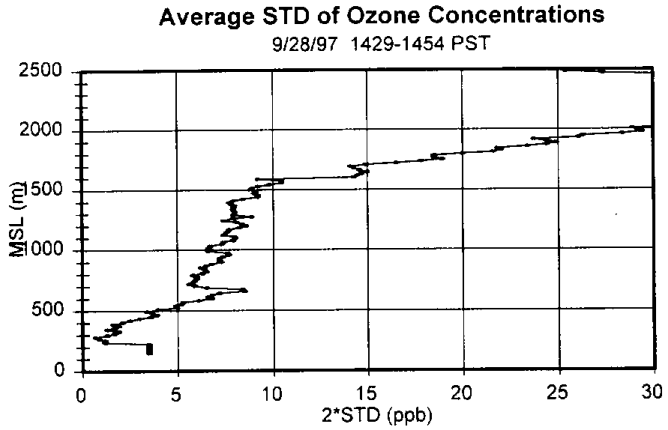

Figure D

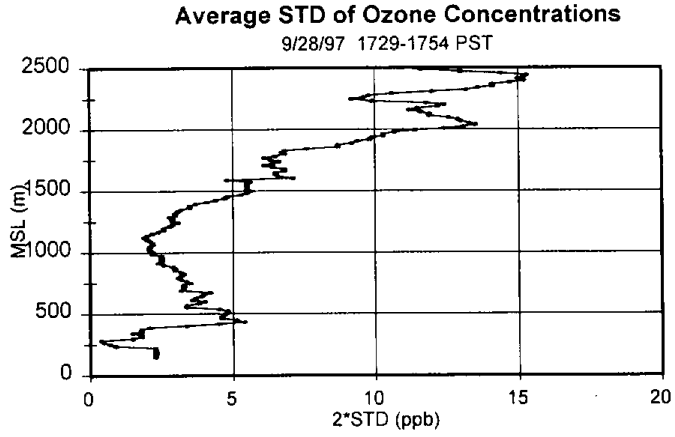

Figure E

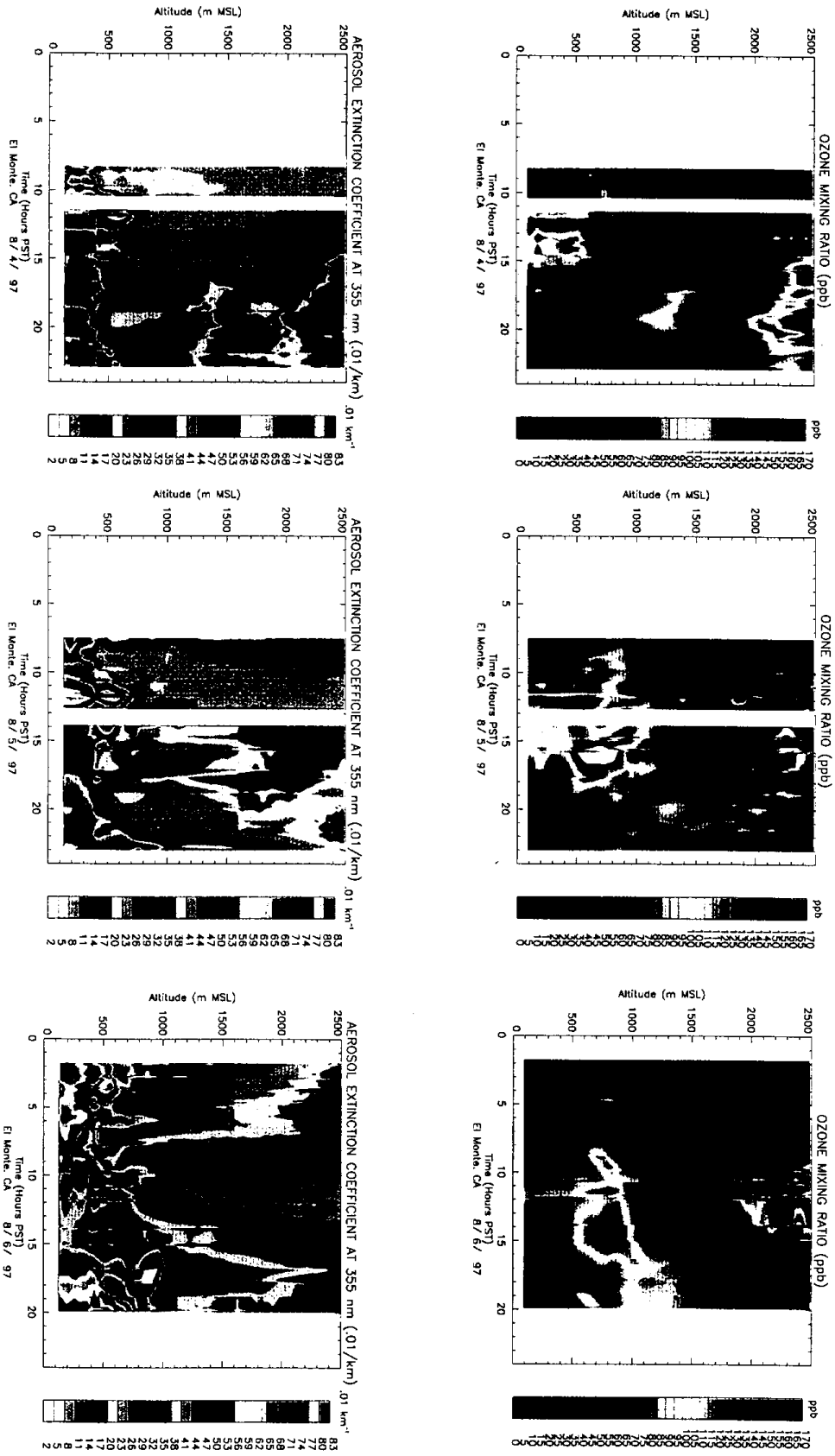

Fig. 1 Time-height charts of ozone and aerosol during the episode of August 4-6, 1997

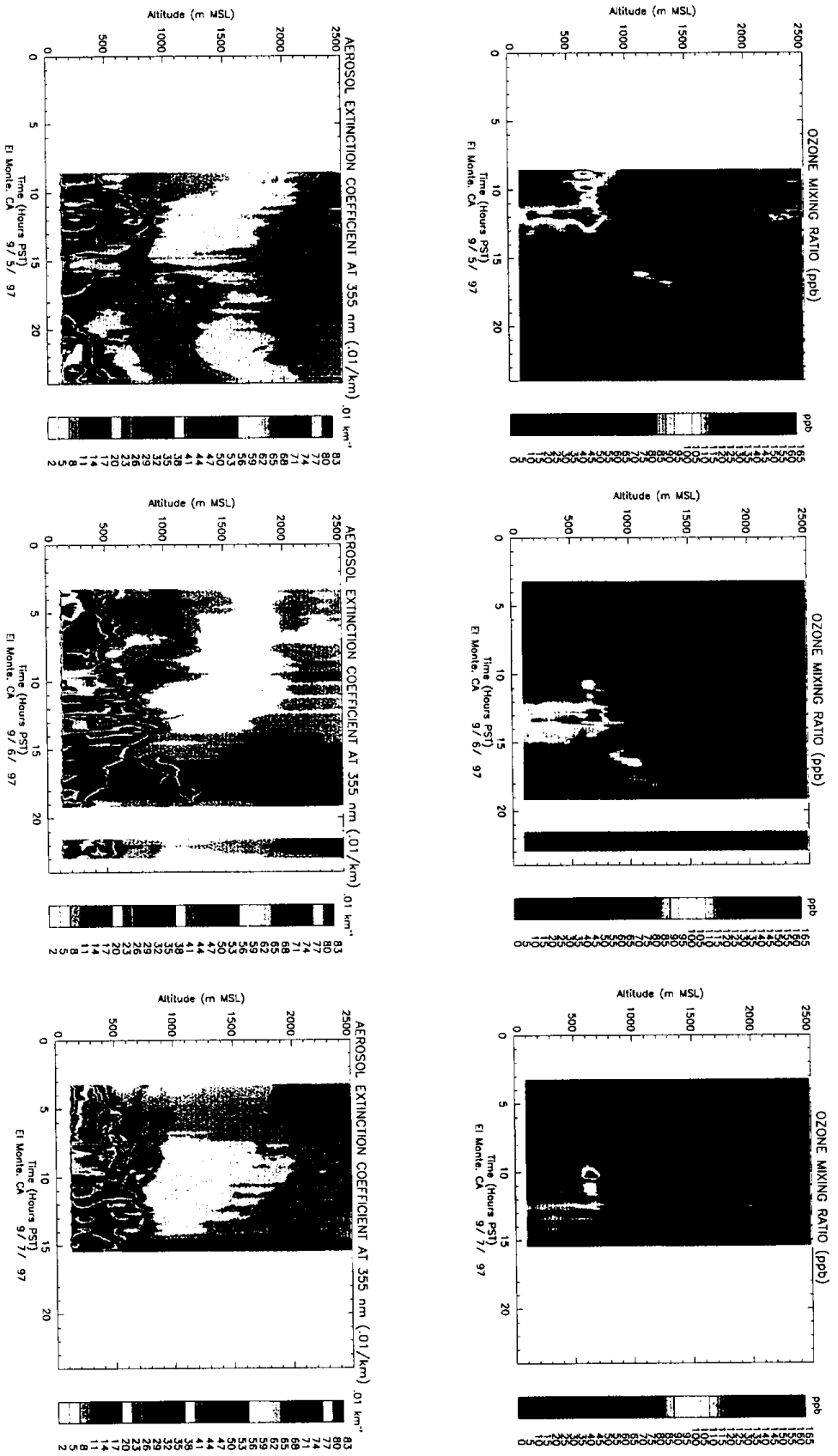

Fig. 2 Time-height charts of ozone and aerosol during the episode of September 3-7, 1997

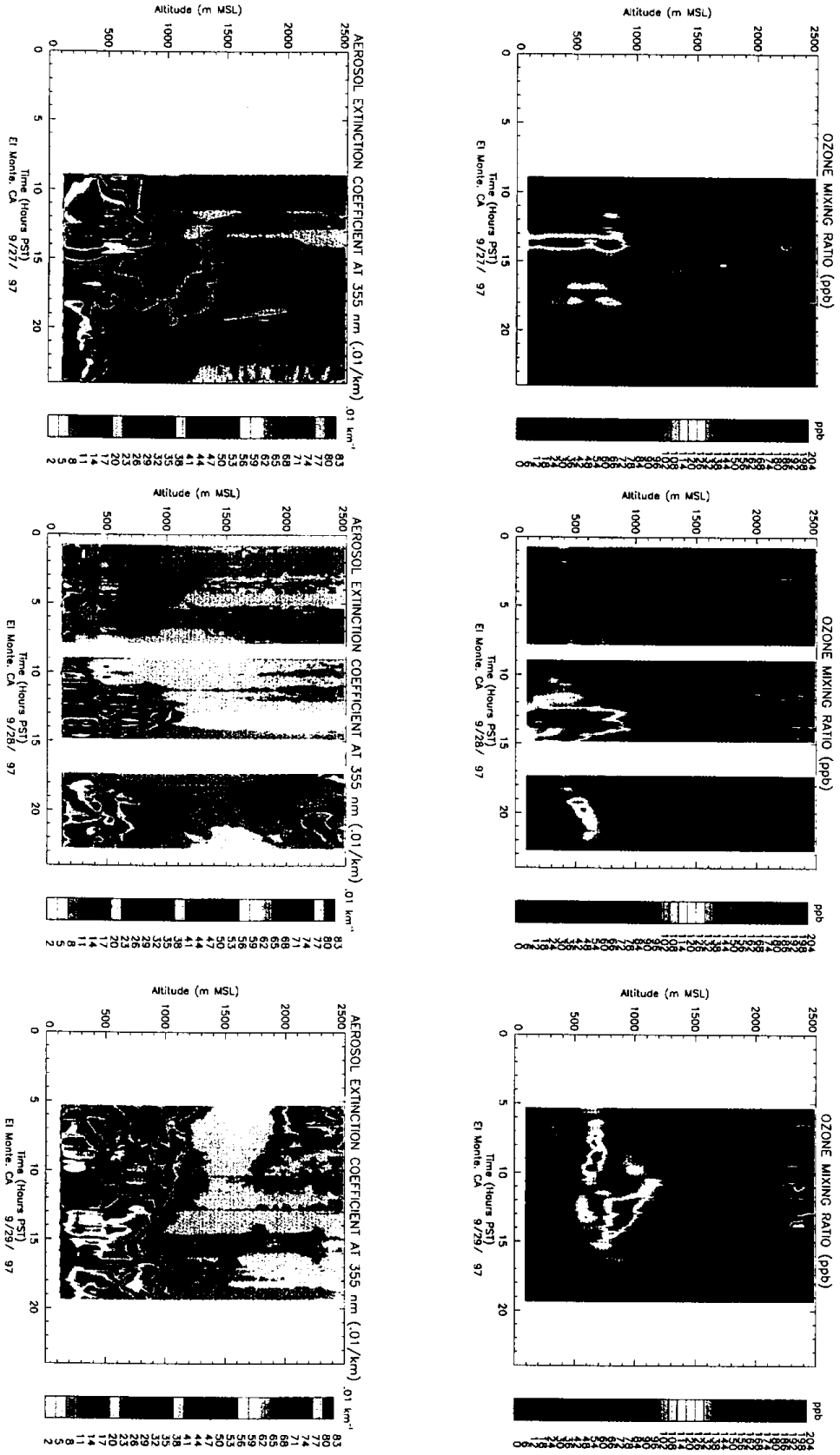

Fig. 3 Time-height charts of ozone and aerosol during the episode of September 27-29, 1997

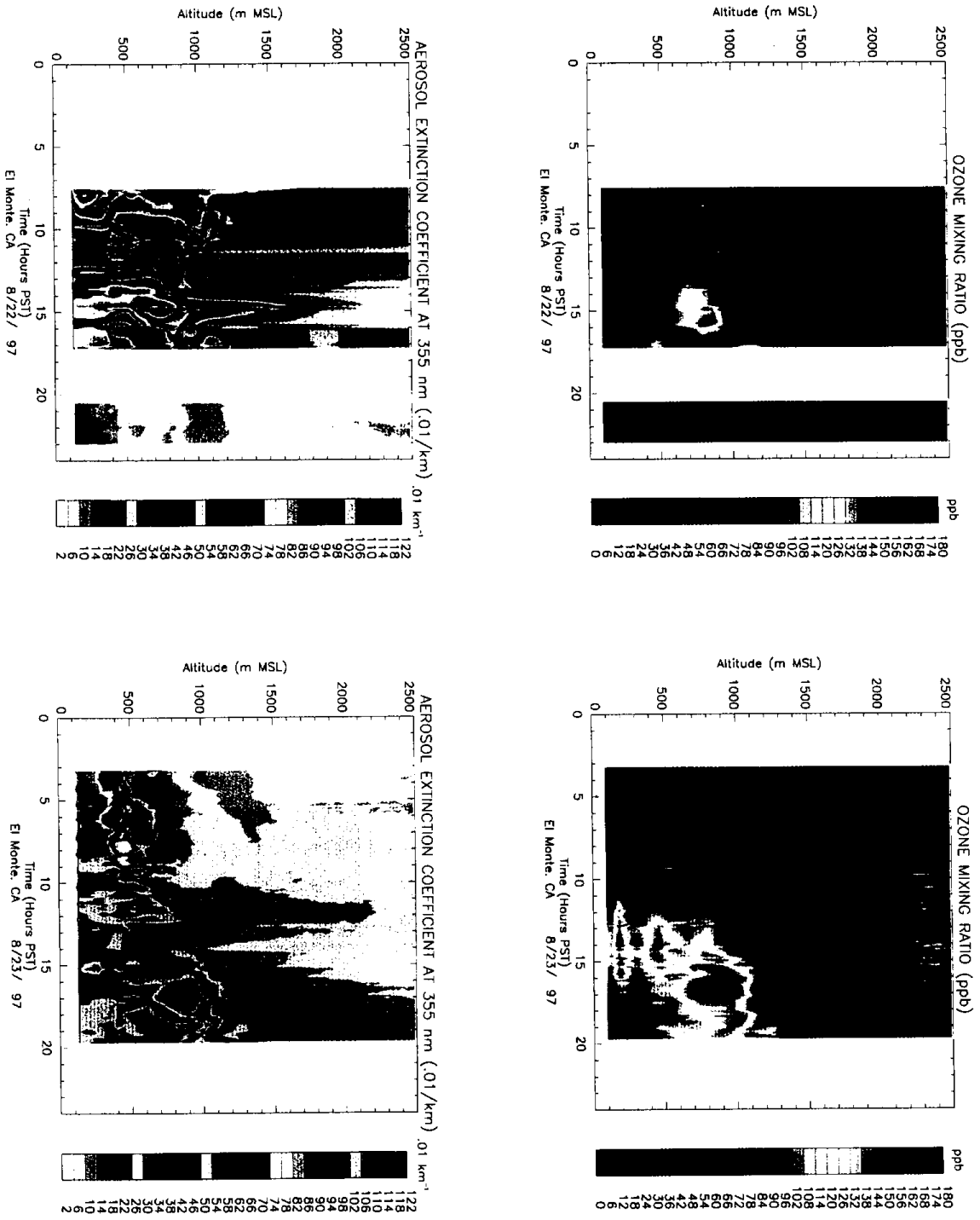

Fig. 4 Time-height charts of ozone and aerosol during the episode of August 22-23, 1997

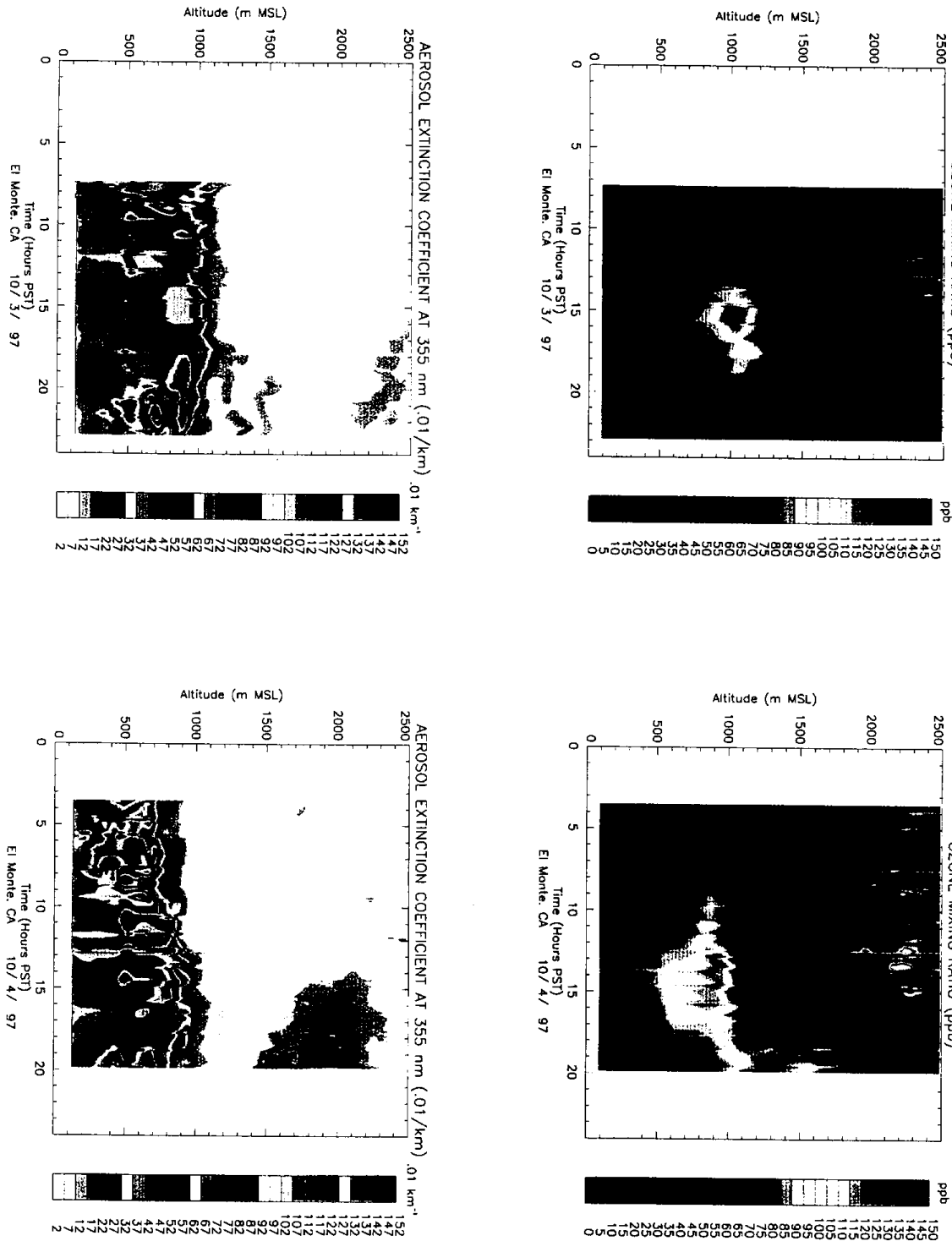

Fig. 5 Time-height charts of ozone and aerosol during the episode of October 3-4, 1997

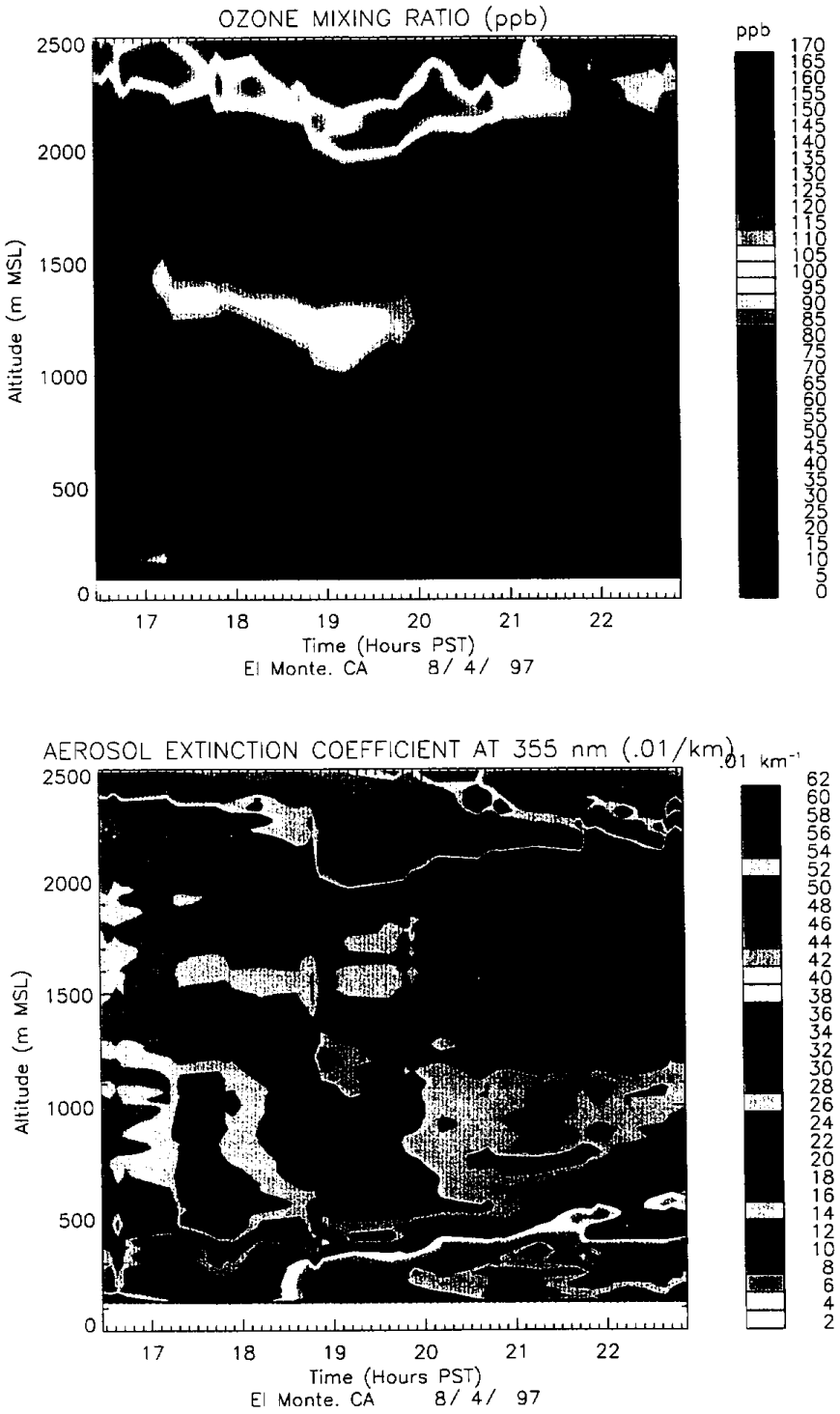

Fig. 6 Time-height charts of ozone concentrations and aerosol extinction coefficients in the evening of August 4

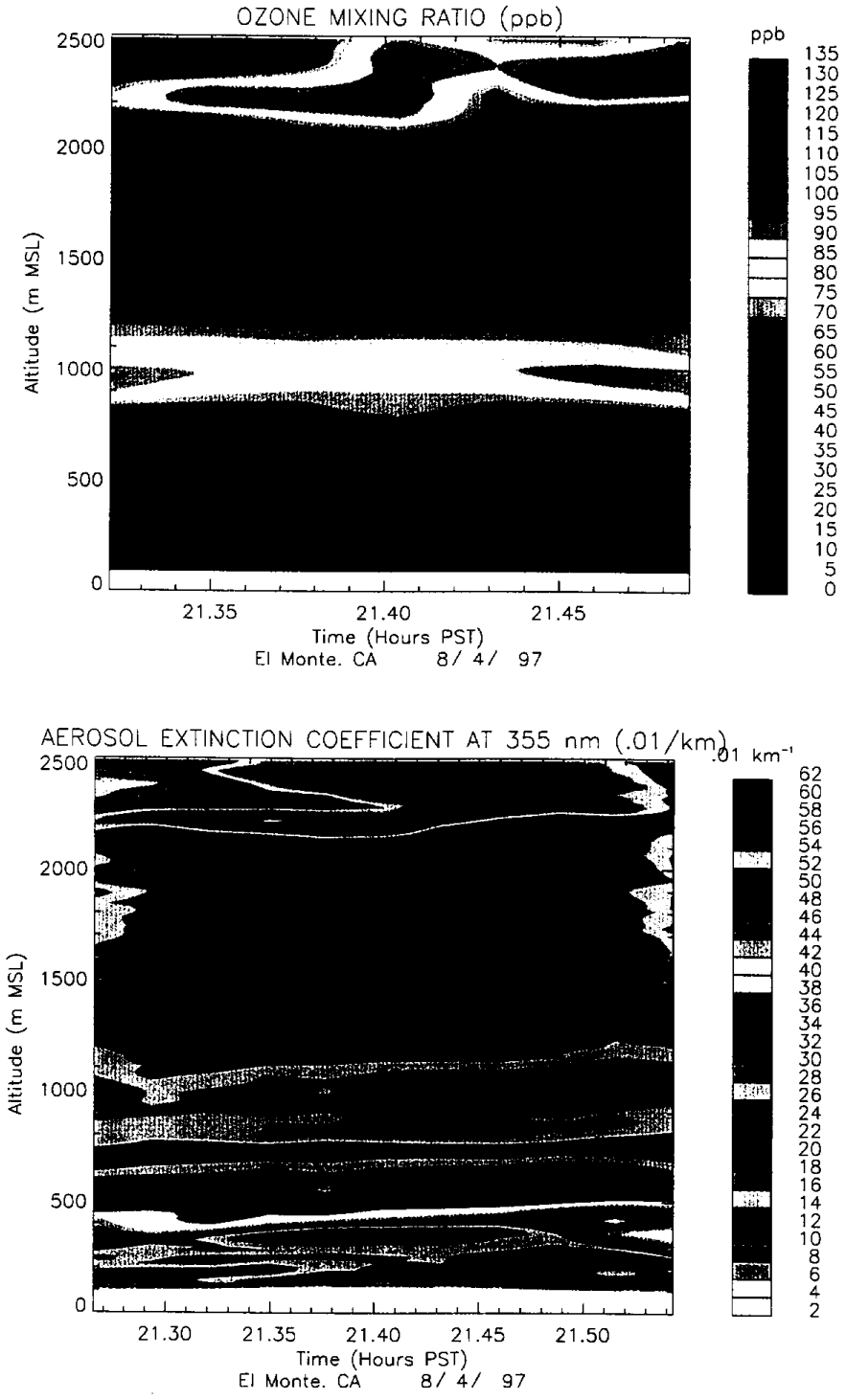

Fig. 7 Time-height chart of ozone concentrations and aerosol extinction coefficients during one scanning at about 2120 PST on August 4, 2997

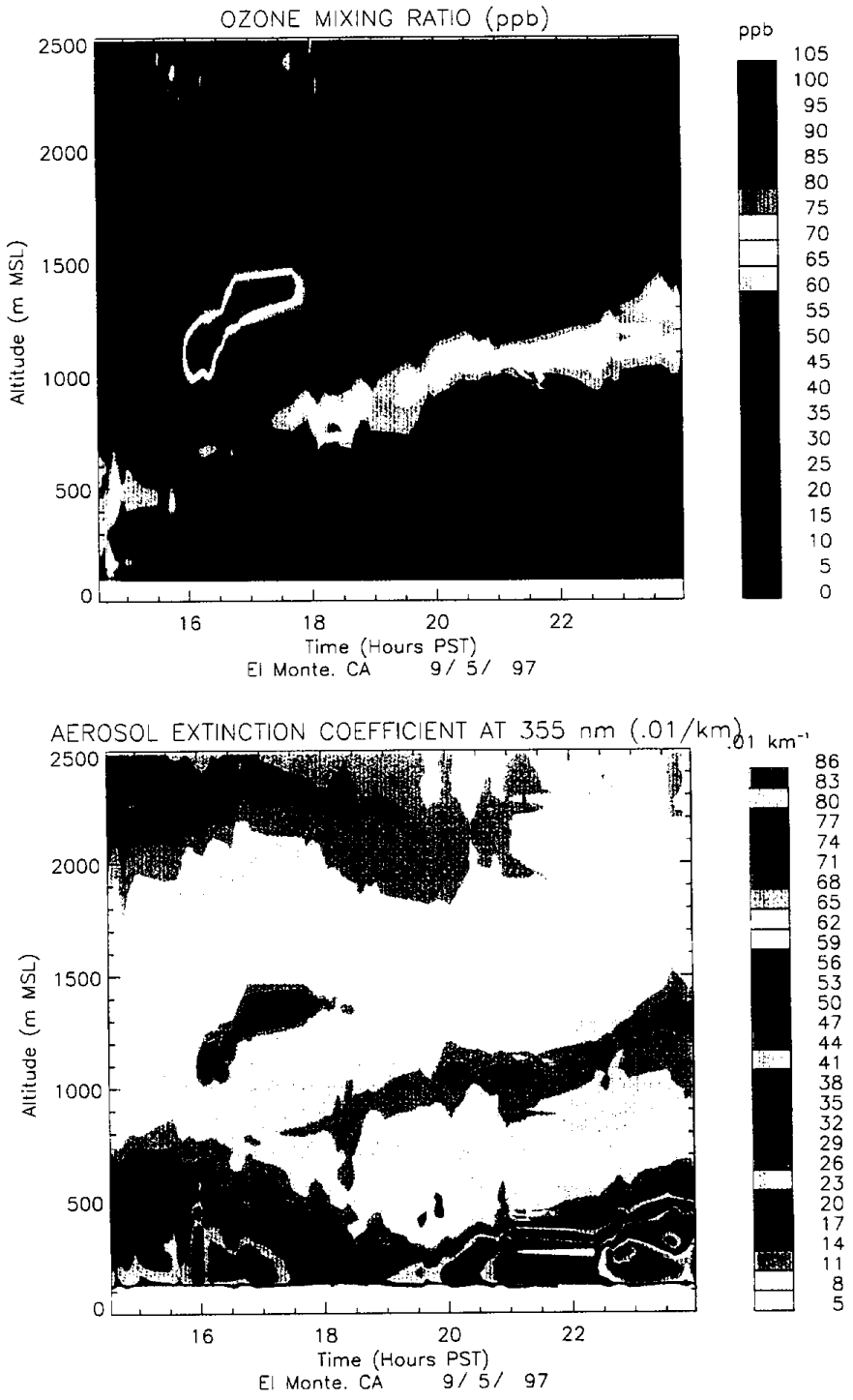

Fig. 8 Time-height charts of ozone concentrations and aerosol extinction coefficients from late afternoon to evening on September 5, 1997

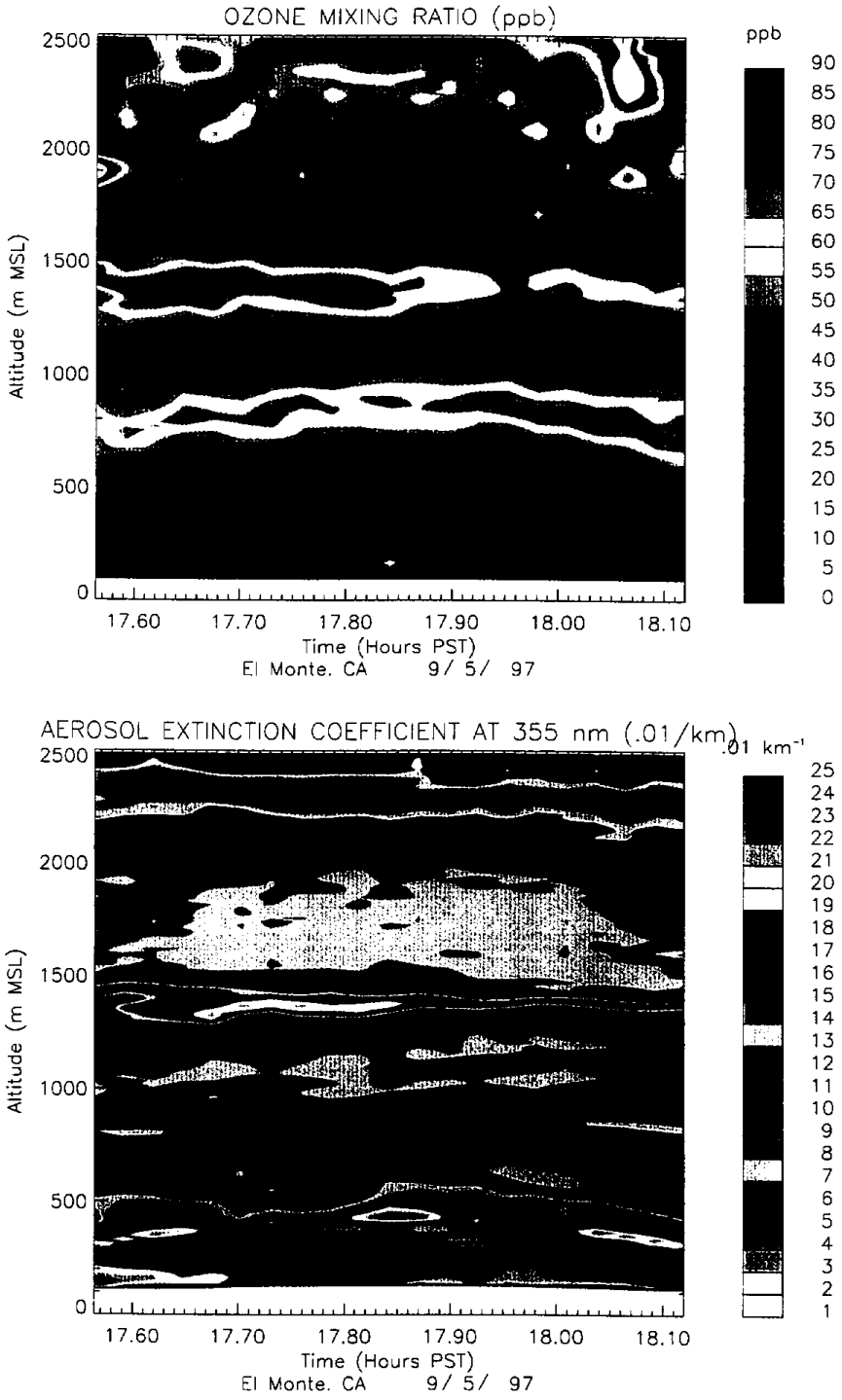

Fig. 9 Time-height chart of ozone concentrations and aerosol extinction coefficients during one scanning at about 1800 PST on September 5, 1997

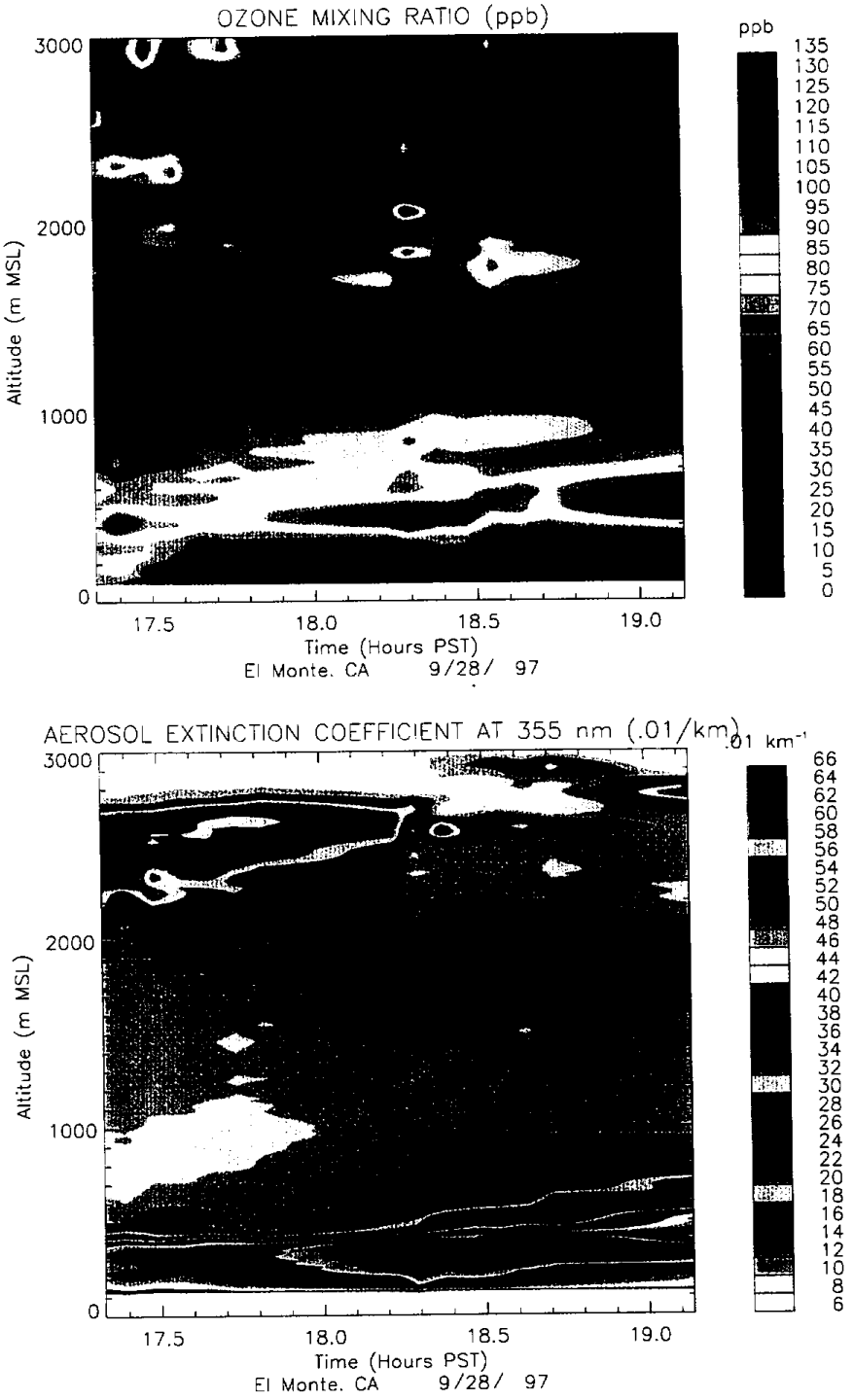

Fig. 10 Time-height charts of ozone concentrations and aerosol extinction coefficients in the evening on September 28, 1997

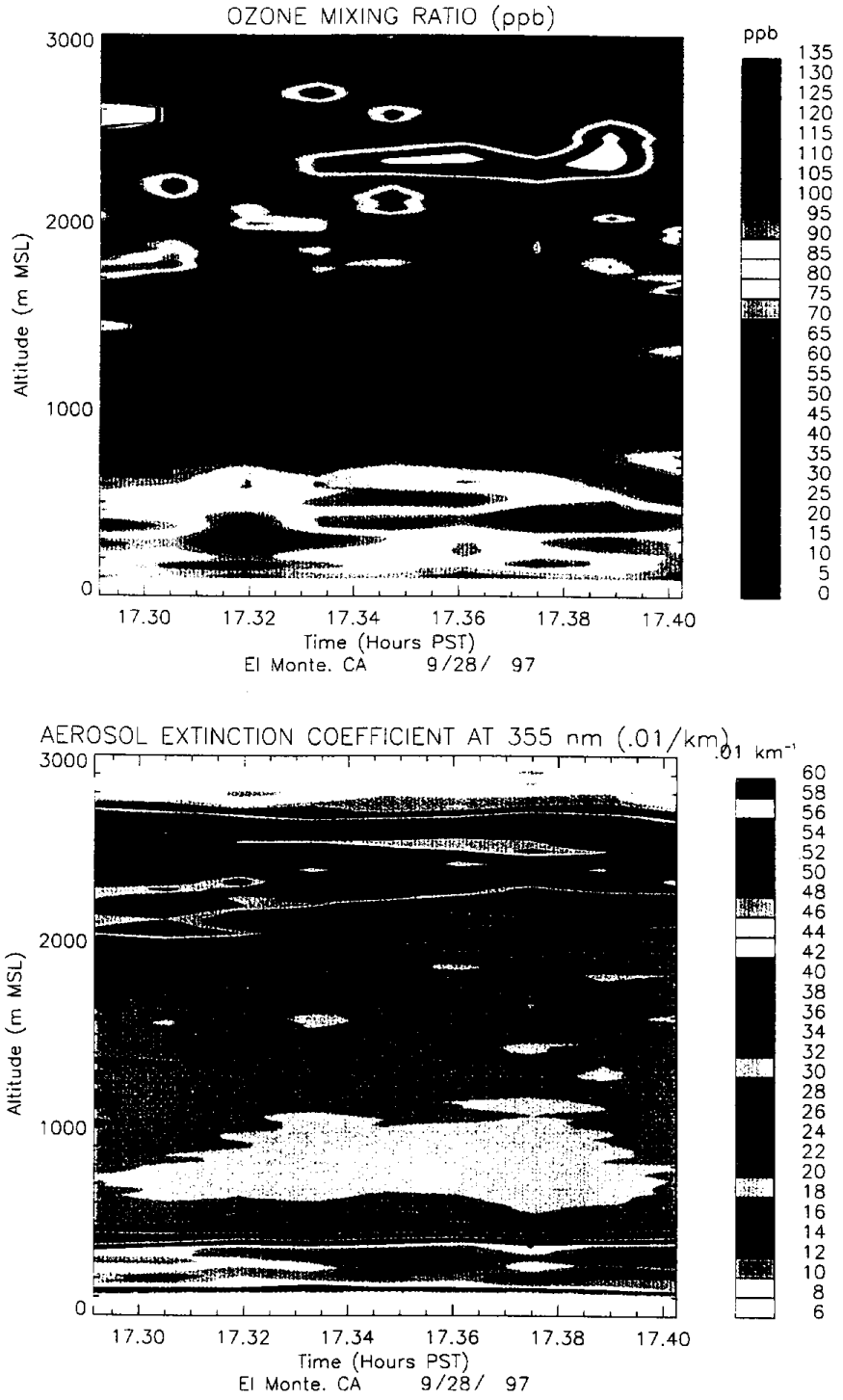

Fig. 11 Time-height chart of ozone concentrations and aerosol extinction coefficients during one scanning at about 1720 PST on September 28, 1997

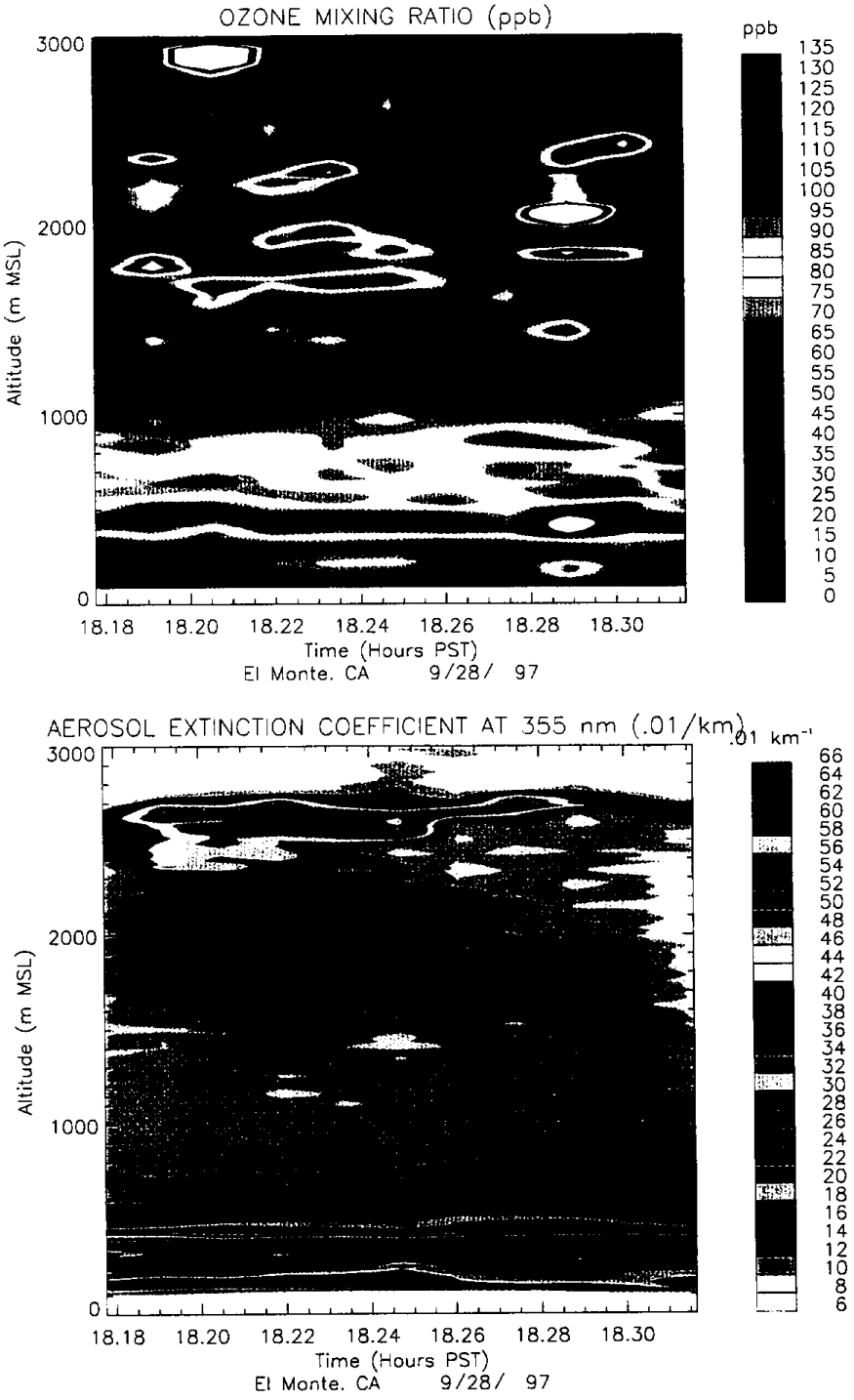

Fig. 12 Time-height chart of ozone concentrations and aerosol extinction coefficients during one scanning at about 1820 PST on September 28, 1997

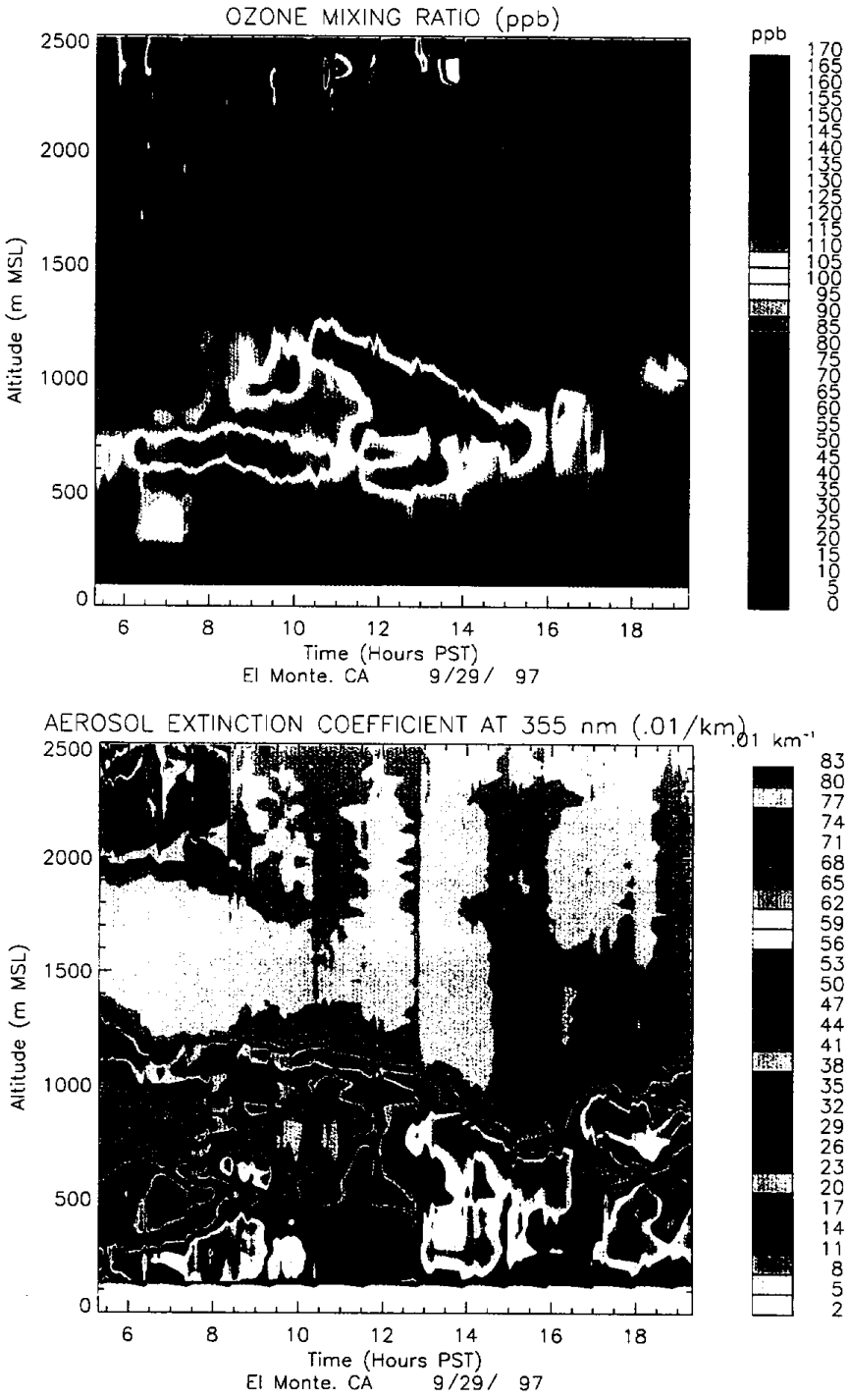

Fig. 13 Time-height charts of ozone concentrations and aerosol extinction coefficients September 29, 1997

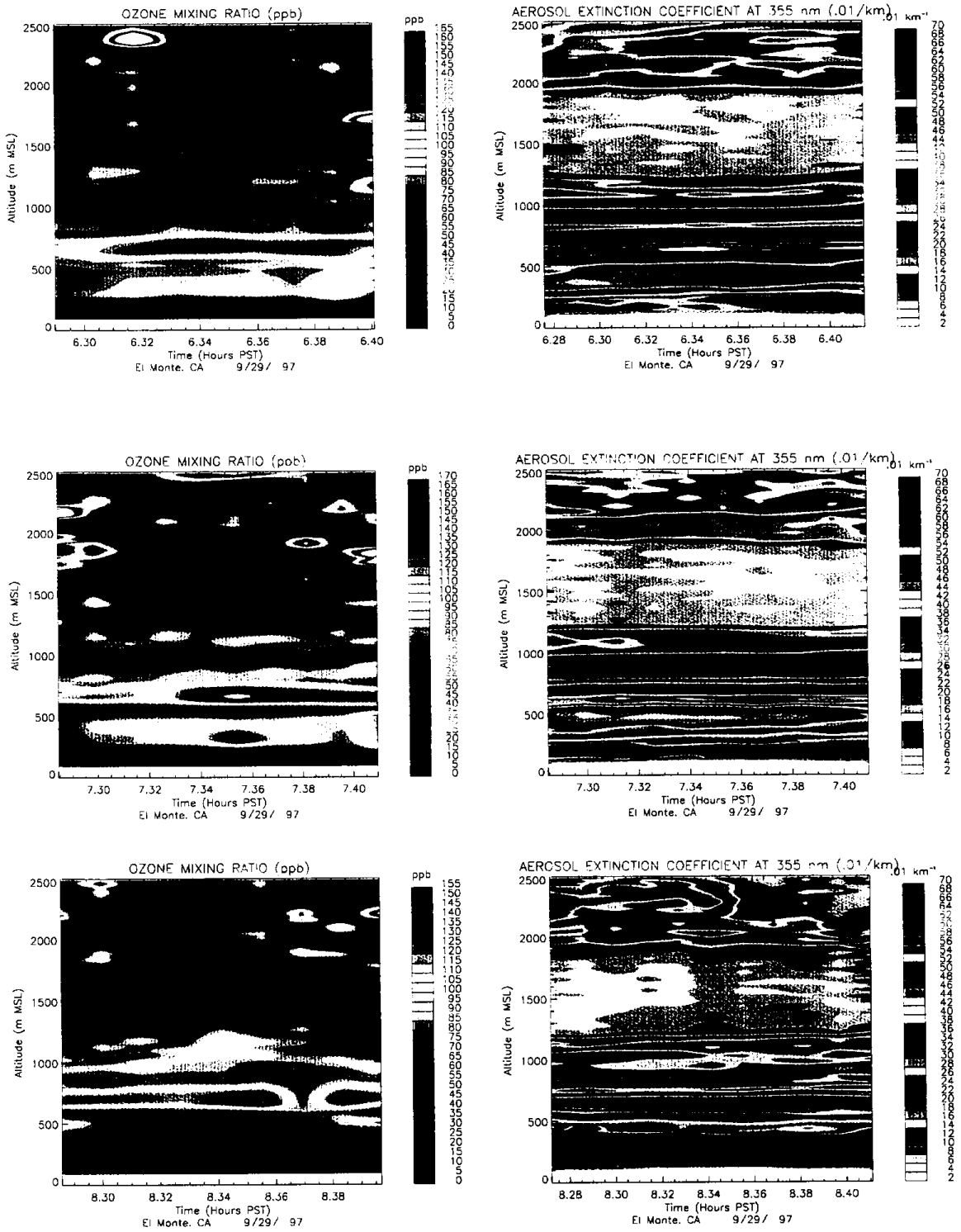

Fig. 14 Time-height charts of ozone concentrations and aerosol extinction coefficients in three scanning operations at about 0620, 0720, and 0820 PST on September 29, 1997